frontiers | Frontiers in Earth Science

ORIGINAL RESEARCH
published: 13 June 2022
doi: 10.3389/feart.2022.885602

Effect of Diagenesis on the Quality of Sandstone Reservoirs Exposed to High-Temperature, Overpressure, and CO_2-Charging Conditions: A Case Study of Upper Miocene Huangliu Sandstones of Dongfang District, Yinggehai Basin, South China Sea

Xiaowei Lv[1,2,3], Meiyan Fu[1,2]*, Shaonan Zhang[4], Xianghao Meng[1,2], Yi Liu[5], Xiaoqi Ding[1,2], Ya Zhang[6] and Tengjiao Sun[1,2]*

[1]College of Energy Resource, Chengdu University of Technology, Chengdu, China, [2]State Key Laboratory of Oil and Gas Geology and Exploitation, Chengdu, China, [3]The Research Institute of Henan Oilfield Company, SINOPEC, Zhengzhou, China, [4]College of Geosciences and Technology, Southwest Petroleum University, Chengdu, China, [5]The Research Institute of Zhanjiang Branch of CNOOC, Zhanjiang, China, [6]Southwest Oil and Gas Field Company of Petro China Company Limited, Chengdu, China

OPEN ACCESS

Edited by:
Wenlong Ding,
China University of Geosciences, China

Reviewed by:
Lanpu Chen,
China University of Geosciences Wuhan, China
Duan Wei,
China University of Geosciences, China

***Correspondence:**
Xiaowei Lv
lxwcdut@163.com
Meiyan Fu
fumeiyan08@cdut.cn

Specialty section:
This article was submitted to Structural Geology and Tectonics, a section of the journal Frontiers in Earth Science

Received: 28 February 2022
Accepted: 03 May 2022
Published: 13 June 2022

Citation:
Lv X, Fu M, Zhang S, Meng X, Liu Y, Ding X, Zhang Y and Sun T (2022) Effect of Diagenesis on the Quality of Sandstone Reservoirs Exposed to High-Temperature, Overpressure, and CO_2-Charging Conditions: A Case Study of Upper Miocene Huangliu Sandstones of Dongfang District, Yinggehai Basin, South China Sea. Front. Earth Sci. 10:885602. doi: 10.3389/feart.2022.885602

The Upper Miocene Huangliu sandstones of the Dongfang district are currently regarded as an important exploration target in the Yinggehai Basin. Affected by the anomalous diagenetic environments of high temperature, overpressure, and CO_2 fillings, the diagenetic evolution of the Huangliu sandstones appear complicated characteristics and subsequently exert a significant influence on reservoir development. Integrated methods employed in this study include an electron microscope, cathode luminescence, X-ray diffraction, scanning electron microscope, electron microprobe, stable isotope analysis, homogenization temperature, and physical property tests. By the comparative researches between the AF-1 and AF-2 areas of the Dongfang district, the aim of this study is to investigate the complex diagenetic modifications and their controlling effects on reservoir quality and development mechanism. With similar sedimentary features, the reservoirs in the AF-1 area exhibit slightly higher porosity than those of the AF-2 area. The permeability in the AF-1 area shows one or two orders of magnitude lower than that of the AF-2 area, and throats size distribution act as a critical factor to cause distinct diversities of permeability. In the AF-1 area, the later appearance of overpressure contributed to stronger compaction intensity and more loss of primary porosity. The dissolution induced by CO_2-rich thermal fluids in late stage enhanced the secondary porosity significantly and improved the total porosity. However, extensive dissolution cause abundant precipitation including carbonate cement and authigenic illite in a closed diagenetic system, which lead to the decrease of reservoirs' permeability. As for the AF-2 area, earlier occurrence of overpressure restrained mechanical compaction obviously and further retarded corrosion of organic acid, which preserved high proportions of primary porosity. Due to lesser impact by CO_2 filling, the AF-2 area had a poor intensity of

dissolution and cementation, and the authigenic illitization was also restrained significantly, which effectively prevented heavy damage on reservoir quality, and especially for permeability. Based on the diagenetic evolution pathways, two types of porosity evolution patterns are established. The effect degree on diagenesis by high temperature, overpressure, and CO_2 filling vary significantly between the AF-1 and AF-2 areas. The two areas show different pathways of diagenetic evolution, forming two development patterns and exhibiting different reservoir types.

Keywords: Huangliu sandstones, high temperature, overpressure, CO_2 dissolution, diagenetic evolution

1 INTRODUCTION

As most of hydrocarbon resources in shallow layers have been discovered and exploration technologies progress continuously, the exploration transferring to deeply buried and complex reservoirs become an inevitable choice, and deepening understandings on the impact for reservoir quality by high pressure, high temperature (HPHT), and CO_2 injection are considered to be even more significant for diminishing prospecting risk in deeper targets (Taylor et al., 2010; Stricker et al., 2016; Duan et al., 2020). Being different from normal pressure coefficient and geothermal gradient, the sandstones exposed in anomalous settings of HPHT and CO_2 filling present a wide variety of diagenetic modifications and complex diagenetic evolution, and consequently exert a battery of crucial controls on reservoir quality and development mechanism (Di Primio and Neumann, 2008; Nguyen et al., 2013; Grant et al., 2014; Fu et al., 2016; Duan et al., 2020; Li et al., 2020).

The important influence of overpressure on reservoir development have been widely studied across the overpressed petroliferous basins worldwide in the last few decades (e.g., Taylor et al., 2010; Grant et al., 2014; Sathar and Jones, 2016; Lai et al., 2017; Santosh and Feng, 2020). The opinion of reducing vertical effective stress (VES) toward intergranular and cement-grain contacts by overpressure is generally accepted, which plays a significant role in primary porosity preservation and subsequently results in anomalously high porosity in deeply buried reservoirs (Osborne and Swarbrick, 1999; Bloch et al., 2002; Tingay et al., 2009; Sathar and Jones, 2016; Li, 2021). Furthermore, considerable studies indicate that overpressure has a non-ignorable influence on several diagenetic aspects mainly as follow: protecting dissolved porosities (Taylor et al., 2015; Zhang et al., 2020; Wang and Wang, 2021), indirectly controlling dissolution efficiency of organic acids and CO_2 (Jansa and Noguera Urrea, 1990; Wilkinson et al., 1997; Duan et al., 2018), retarding clay minerals transformation (Colten-Bradley, 1987; Meng et al., 2012), and affecting cementation intensity such as quartz overgrowth and carbonate cements (Osborne and Swarbrick, 1999; Bloch et al., 2002; Duan et al., 2018).

Temperature is also one of critical factors for reservoir evolution by altering the rate of water–rock reaction and intensity of diagenesis (Schmoker and Gautier, 1988; Di Primio and Neumann, 2008; Yoshida and Santosh., 2020; Zheng et al., 2020; Yang et al., 2021). Previous practical studies show that the high-temperature setting, especially higher geothermal gradient or anomalously thermal events caused by thermal fluid activities, are mostly suggested to have significant effect on enhancing compaction rate, strengthening cementation and dissolution, and accelerating transformation efficiency of clay minerals, which are of great significance to deepen the understanding for formation mechanism of reservoir (Stricker et al., 2016; Dong et al., 2020; Lan et al., 2021; Li, 2022).

In recent years, interest has been increasing on exploring the diagenetic evolution and formation mechanism of sandstone reservoirs influenced by fillings of CO_2-rich thermal fluid (Wilkinson et al., 2009; Fu et al., 2016; Duan et al., 2018; Zhang et al., 2019; Zhao et al., 2020). The CO_2 charging correlated with thermal fluid cause exceptional diagenetic alteration of dissolution and precipitation exert a non-negligible influence on and diagenetic modifications and reservoir development (Watson et al., 2004; Higgs et al., 2007; Zuo et al., 2019; Duan et al., 2020).

There is no single diagenetic element that is solely or dominantly governing the porosity evolution (Mansurbeg et al., 2008; Wang et al., 2020). Most previous studies assessed the effect of diagenesis on reservoir development influenced by one or two of abnormal diagenetic elements including HPHT and CO_2 injection. Fewer work synthetically documented the combined effects for reservoirs quality controlled by multivariate overlapped extreme conditions of HPHT and CO_2 filling in spatial and temporal scale, and the integrated effects controlled by the extreme conditions are barely investigated and poorly understood. The Dongfang district is located at the northern of the central depression in the Yinggehai Basin (**Figure 1A**), of which the Huangliu Formation (N_1h) is a critical exploration target (Xie et al., 2012; Duan et al., 2020). Exposed in anomalous environments characterized by higher pressure coefficient, higher thermal gradient, and CO_2 filling, the Huangliu sandstones have undergone complicated diagenetic history and evolution processes, which provide an excellent opportunity to investigate the complex formation mechanism of reservoirs controlled by HPHT and CO_2 charging. The effect of high temperature, high pressure, and CO_2 filling are studied individually by several published studies in the Dongfang district, yet the integrated impact of the anomalous environments are rarely explored. Utilizing integrated methods of reservoir geology and geochemistry, this study aims to investigate various diagenetic modifications controlled by HPHT and CO_2 charging and unravel the formation mechanisms for the reservoirs of the Huangliu sandstones. By

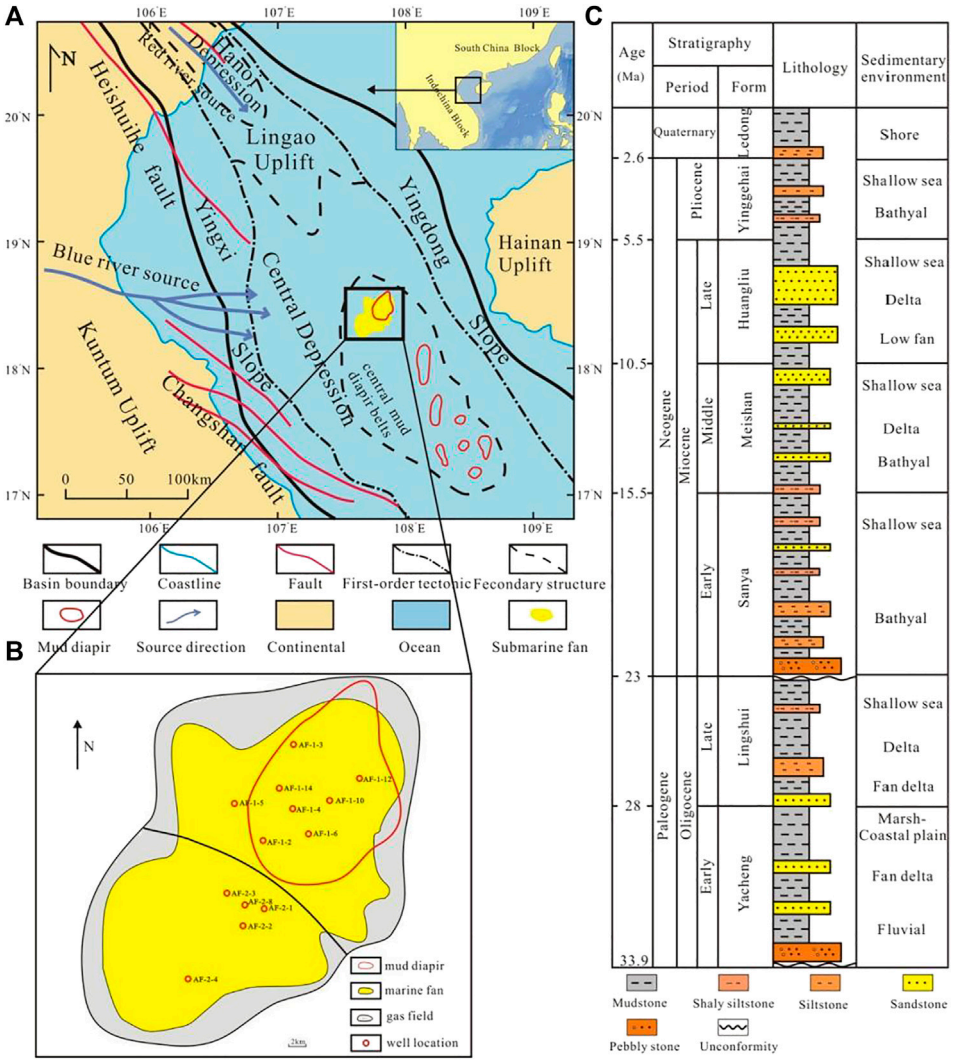

FIGURE 1 | (A) Geographic location of the Yinggehai Basin and the study area. **(B)** Distribution of prospecting wells in the Dongfang district. **(C)** Stratum system of the Dongfang district. (Panel 1A and Panel 1B are modified from Huang et al., 2017; Panel 1C is modified from Duan et al., 2020).

comparative study between the AF-1 and AF-2 areas, the evolution history of porosity and the origin of different distribution tendency of permeability are also discussed. This study case provides valuable insights for understanding the evolution of reservoir quality in the Yinggehai Basin, as well as for similar plays worldwide.

2 GEOLOGICAL SETTING

The Yinggehai Basin is a Cenozoic petroliferous basin developing on the basement of northwestern continental shelf of the South China Sea, with an area of approximate 12×10^4 km^2 (Huang et al., 2017) (**Figure 1A**). With a transform-extensional origin, the basin evolved in accordance with regional lithosphere extension induced by strike-slip movement of the Red River Fault zone (Luo et al., 2003). The basin is generally segmented into three first-order tectonic units: the Yingxi Slope, the Central Depression, and the Yingdong Slope (**Figure 1A**). The Yinggehai Basin is dominated by rapid subsidence and sedimentation rates and accumulates thick-bedded sediments up to 17-km thick (Hao et al., 2000). From bottom to top, the stratigraphic system of the basin mainly contain the Oligocene Yacheng and Lingshui formations; the Miocene Sanya, Meishan, and Huangliu formations; the Pliocene Yinggehai Formation; and the Quaternary Ledong Formation (**Figure 1C**) (Duan et al., 2020). The main source rocks layers are made up of dark gray marine mudstone from supper Sanya Formation and Lower Meishan Formation (Xie et al., 2012). The sandstone- or siltstone-dominated layers associated with deltic or gravity flow deposits in the Huangliu and Yinggehai formations constitute the principal reservoirs (Xie et al., 2012). The basin-scale thick mudstone sequences of overlying Yinggehai Formation mainly act as effective gas-bearing seal (Xie et al., 2012).

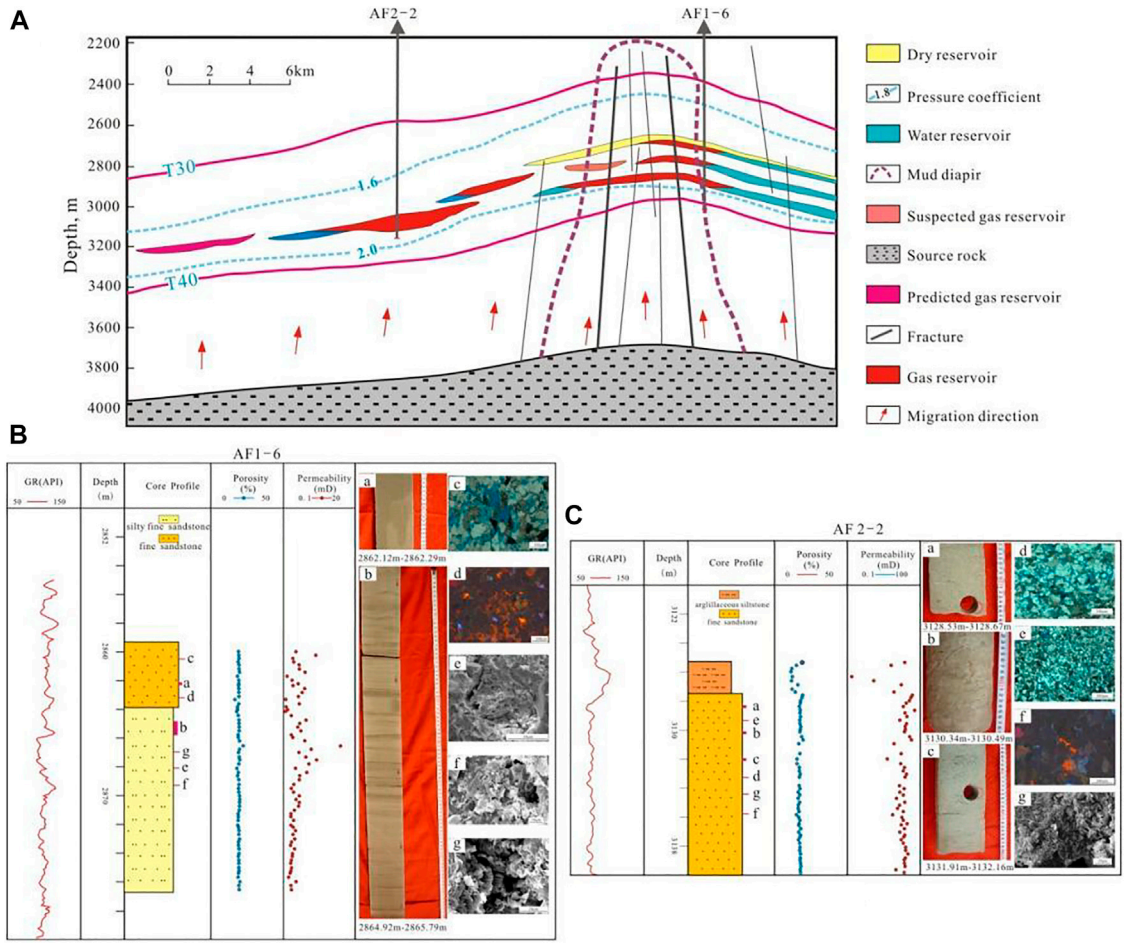

FIGURE 2 | Accumulation model of natural gas accumulation related to mud diapir in the Dongfang district in the Yinggehai Basin **(A)** (modified from Xie et al., 2012). The comprehensive profile comprising logging characteristics, lithology, physical properties, and photographs of cores and diagenetic alterations in well AF-1–6 **(B)** and well AF-2–2 **(C)** in the Dongfang district.

In the Yinggehai Basin, the intensive extension of lithosphere and simultaneous upwelling of asthenosphere are mainly responsible for high geothermal gradient, with an average geothermal gradient of 4.6°C/100 m (Hao et al., 2000). The extensive undercompaction of thick-bedded accumulation of mudrock caused by rapid deposition rate contributes to the generation of overpressure in medium–deep layers (Fu et al., 2016). The hydrocarbon generation and thermal expansion of pore fluids further enhance overpressure (Hao et al., 2000), and the allogenic transmission conducted by episodic fracture opening is also considered as a non-negligible mechanism for heightening overpressure (Luo et al., 2003). The overpressure prevails mostly in the central depression with maximum pressure coefficient of 2.2, and the depth of top boundary of overpressure zone increase from the center to the margin of the basin (Duan et al., 2018). Triggered by extensional stress from strike-slip movement and overpressured plastic mudstone, multicolumn diapirs were developed in the central depression (Hao et al., 2000). With diapir intrusion, the thermal fluid invaded toward the overlying strata, accordingly heightening the geothermal field and pressure field (Hao et al., 2000).

The Dongfang district is one of the principal gas fields in the Yinggehai Basin, with an area of about 2,400 km^2 (**Figure 1B**). The fine-grained sandstones and silty sandstones of the Huangliu Formation are main gas-bearing in the Dongfang Gas Field, which are identified to derive from shallow marine gravity flow with main provenance from Blue River (Huang et al., 2019). Multiple sets of sandy lobes serve as the principal bodies of the Huangliu sandstones, which deposit as multi-period alterations of gravity flow (Huang et al., 2019) (**Figures 2B,C**). The minor part of the eastern AF-1 area with very fine-grained sandstones is determined as neritic sandbar deposition with main source from the Hainan Uplift (Huang et al., 2019). Located around the diapir zone, the AF-1 area suffered multi-period episodic injection of CO_2-rich thermal fluid severely (**Figure 2A**) (Fu et al., 2016). In contrast, the AF-2 area lied far away from the diapir and underwent minimal interference from thermal fluid intrusion (**Figure 1B**) (Fu et al., 2016). The present-day formation temperature of Huangliu sandstones

TABLE 1 | Results of natural gas compositions, stable isotope, formation pressure and temperature of wells from drilling tests in the Huangliu sandstones. MDT: modular formation dynamics tester; DST: drill stem testing.

Well	Depth (m)	Testing methods	Natural gas composition (%)			$\delta^{13}C_1$/‰	$\delta^{13}C_{CO2}$/‰	Pressure factor	Temperature(°C)
			CH_4	C_nH_m ($2 \leq n \leq 5$)	CO_2				
AF-1–12	2,792.6–2,806.3	DST	30.36–34.54	0.62–0.96	53.84–56.38	–30.57	–2.67	1.96–2.07	127.4–140.3
AF-1–14	2,914.0–2,959.0	MDT&DST	65.43–73.59	1.66–1.73	18.38–23.46	–31.76	–3.87	1.89–1.92	132.8–143.6
AF-1–2	2,977.3–3,054.6	MDT	—	—	—	—	—	1.87–1.89	129.5–140.7
AF-1–4	2,833.6–2,879.0	MDT&DST	35.18–64.26	1.31–1.39	23.60–53.62	–32.47	–6.19	1.92–1.95	124.0–137.8
AF-1–6	2,815.8–2,863.0	MDT&DST	18.73–22.31	0.34–0.82	71.26–73.85	–35.54	–4.55	1.95–1.98	136.4–137.3
AF-2–1	2,973.2–3,125.3	MDT	88.83–94.26	2.51–3.36	1.36–5.78	–32.34	–15.24	1.75–1.83	129.4–142.1
AF-2–2	3,035.6–3,142.9	MDT	92.53–93.65	2.83–2.89	2.64–3.18	–32.97	–19.66	1.72–1.78	131.8–142.4
AF-2–4	3,215.3–3,441.8	MDT	96.26–97.93	0.14–0.28	1.42–3.43	–32.54	–18.58	1.66–1.72	135.6–148.6

present minor distinction (**Table 1**), but the homogenization temperature of fluid inclusion indicate that the AF-1 area has experienced anomalously higher temperature (112–193°C) than the AF-2 area (66–131°C) in diagenetic history (Hao et al., 2000; Duan et al., 2020). The AF-1 area shows a higher pressure coefficient (1.87–2.07) than that of the AF-2 area (1.66–1.83) (**Table 1**). The CO_2 contents of wells intervals in the AF-1 area (18.38–73.85 vol%) are obviously higher than that of the AF-2 area (1.36–5.78 vol%) (**Table 1**).

3 SAMPLES AND METHODS

To investigate lithofacies and sedimentary structures, 46-m core intervals were observed and depicted from eight wells in total (Wells AF-1–12, AF-1–2, AF-1–3, AF-1–4, AF-1–6, AF-2–1, AF-2–2, and AF-2–8, shown in **Figure 1B**), from which all core plugs and cutting samples were collected and processed to study the petrological feature, diagenetic alteration, and physical properties. All of experiments and analyses were conducted at the State Key Laboratory of Oil and Gas Reservoir Geology and Exploitation, Chengdu, China.

The thin sections (163 samples) were impregnated with blue epoxy resin and stained with alizarin red S and K-ferricyanide to examine pores structure and recognize carbonate cements. A DMAX-3C X-ray diffraction (Rigaku Corporation, Tokyo, Japan) was employed to measure the composition of clay minerals with 118 cutting samples. The cathode luminescence (CL) examinations for 47 samples of polished thin sections were finished using a MK5-2 stage (CITL, Hertfordshire, England), with a voltage of 14 kV, an electric current of 380 μA. To distinguish the genesis of carbonate cements, 15 sandstone samples were examined for stable carbon and oxygen isotope composition, which were completed by a MAT253 isotope ratio mass spectrometer (Thermo Fisher Scientific, Waltham, MA, United States), with a precision of 0.0037‰ for $\delta^{13}C$ and 0.013‰ for $\delta^{18}O$. The results were reported with respect to the Vienna Pee Dee Belemnite (VPDB). The measurements of homogenization temperature fluid inclusions from 22 samples were conducted by a cooling–heating stage of THM600 (Linkam Scientific, Surrey, England). To upgrade the accuracy, every sample analysis was repeated at least three times, with a precision of ± 1°C. To clearly detect the texture of cements and clay minerals, 45 samples were selected with carbon coated for scanning electron microscope (SEM) observation, which were completed by an apparatus of Quanta 250 FEG (FEI Company, Hillsboro, OR, United States) under an acceleration voltage of 20 kV and a filament current of 240 mA. The determinations of elemental composition of cements (12 samples) were conducted by an EPMA-1720 H Series electron probe (Shimadzu Corporation, Kyoto, Japan), with an acceleration voltage of 15 kV and an electric current of 10 nA.

For physical properties investigation, 135 core plugs and 112 core plugs were collected from the AF-1 area and the AF-2 area, respectively. The porosity tests were conducted by a helium porosimeter (UltraPore-300) and permeability analyses were completed by an air-permeability instrument (UltraPerm-400). This study selected five core plugs and two core plugs from the AF-1 area and the AF-2 area, respectively, to research reservoir microstructure. The constant-rate mercury injection was employed to analyze pore-throat size, and an automatic pore structure tester (ASPE-730) was adopted to accomplish the test with a parameter accuracy of 0.001 μm.

4 RESULTS

4.1 Reservoir Characteristics

4.1.1 Petrology Feature

The Huangliu sandstones of the AF-1 area are dominated by very fine- and fine-grained sandstones, mostly classified as lithic quartz sandstones according to classification scheme proposed by Folk (1980) and averaged as $Q_{79.3}$ $F_{6.1}$ $L_{14.6}$. By contrast, the AF-2 area is featured predominantly by feldspar lithic sandstones and slightly coarser grain size, with an average compositional value of $Q_{74.6}$ $F_{9.1}$ $L_{16.3}$. The contents of monocrystalline quartz (av. 51.3%) evidently surpass that of polycrystalline quartz (av. 4.8%), and the proportion of K-feldspar (av. 5.4%) is higher than that of plagioclase (av. 1.2%), and metamorphic lithic fragments (av. 7.7%) is much more richer than volcanic lithic fragments (av. 0.9%). As a whole, the interstitial materials are dominated by detrital and authigenic clay minerals and carbonate cements, with minor siliceous cements. Generally, the Huangliu sandstones are

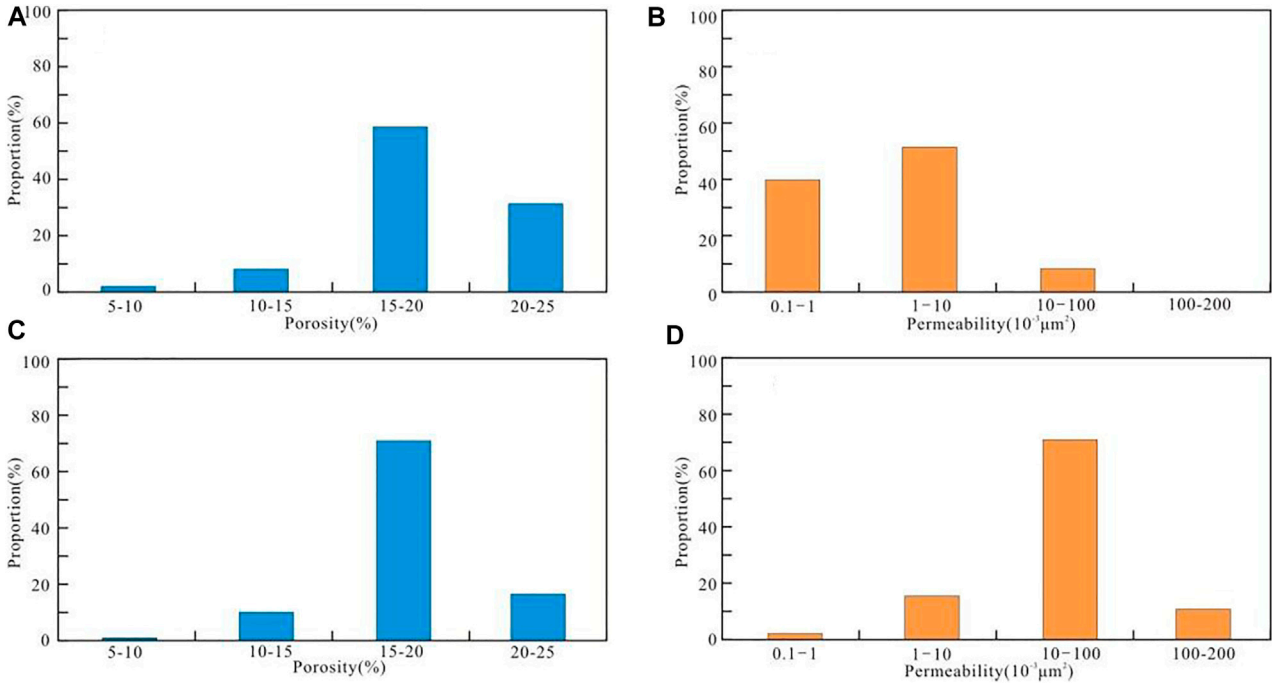

FIGURE 3 | Distribution characteristics of **(A)** the porosity in the AF-1 area, **(B)** permeability in the AF-1 area, **(C)** porosity in the AF-2 area, and **(D)** permeability in the AF-2 area in the Huangliu sandstones.

moderately to well sorted, mainly grain supported, and subangular to subround.

4.1.2 Porosity and Permeability

The average value of porosity in the AF-1 area (18.4%) is slightly higher than that of the AF-2 area (17.9%), with a median distribution span from 14.6% to 22.4% (**Figure 3**). However, the permeability of the Huangliu sandstones in the AF-2 area is dramatically higher than that of the AF-1 area (**Figure 3**). The values of permeability range from 0.1 to 10 mD (81% of total samples) in the AF-1 area and from 10 to 100 mD (72% of total samples) in the AF-2 area (**Figure 3**). Most intervals of the Huangliu sandstones in the AF-1 area belong to medium-porosity and low-permeability reservoirs, while that of the AF-2 area are mainly ranked as medium-porosity and medium-permeability reservoirs.

4.1.3 Microscopic Pore Structures

The measurements by constant-rate mercury injection show that the distribution tendency of pore radii presents a smaller difference between the samples of the AF-1 area and the AF-2 area (**Figure 4A**). However, the performance of pore-throats radii distribution reveals prominent distinction: the dominated extent of samples from the AF-1 area range from 0.5 to 2.3 μm while that of the AF-2 area range from 4.2 to 5.5 μm (**Figure 4B**). Correspondingly, from the perspective of physical properties, the samples from the AF-1 area show low permeability, and those of the AF-2 area display medium permeability.

4.2 Diagenesis

In the Dongfang district, the combinations of anomalous geothermal field, pressure, and thermal fluid, present considerable heterogeneous distributions in time and space, which control diagenetic alterations significantly and result in a wide variety of responses on authigenic minerals and pore-throat microstructure.

4.2.1 Compaction

The mechanical compaction can be observed ubiquitously in the Huangliu sandstones, which are visibly confirmed with bended strip-shaped minerals and deformation of ductile fragments (**Figures 5A,B**). The types of grains contacts mostly center on planar and spot-line and concavo-convex contacts is subordinate, whereas the pressure solution of framework grains is almost unobservable (**Figures 5A,B**). The measured porosities can still maintain 19–23% than expected at the equivalent buried depth of 2800–3000 m. The anomalous variations of porosity–depth trend deviating from routine situation indicate that compaction degree is relatively weaker, which facilitate the preservation of primary porosity.

4.2.2 Cementation

4.2.2.1 Carbonate cements

The carbonate cements in the Huangliu sandstones mainly consist of siderite, calcite, ferrocalcite, dolomite, and ankerite, and present multistage geneses and regional variations. The total amounts of carbonate cements in the AF-1 area are significantly higher than that of the AF-2 area (**Table 2**). The carbonate

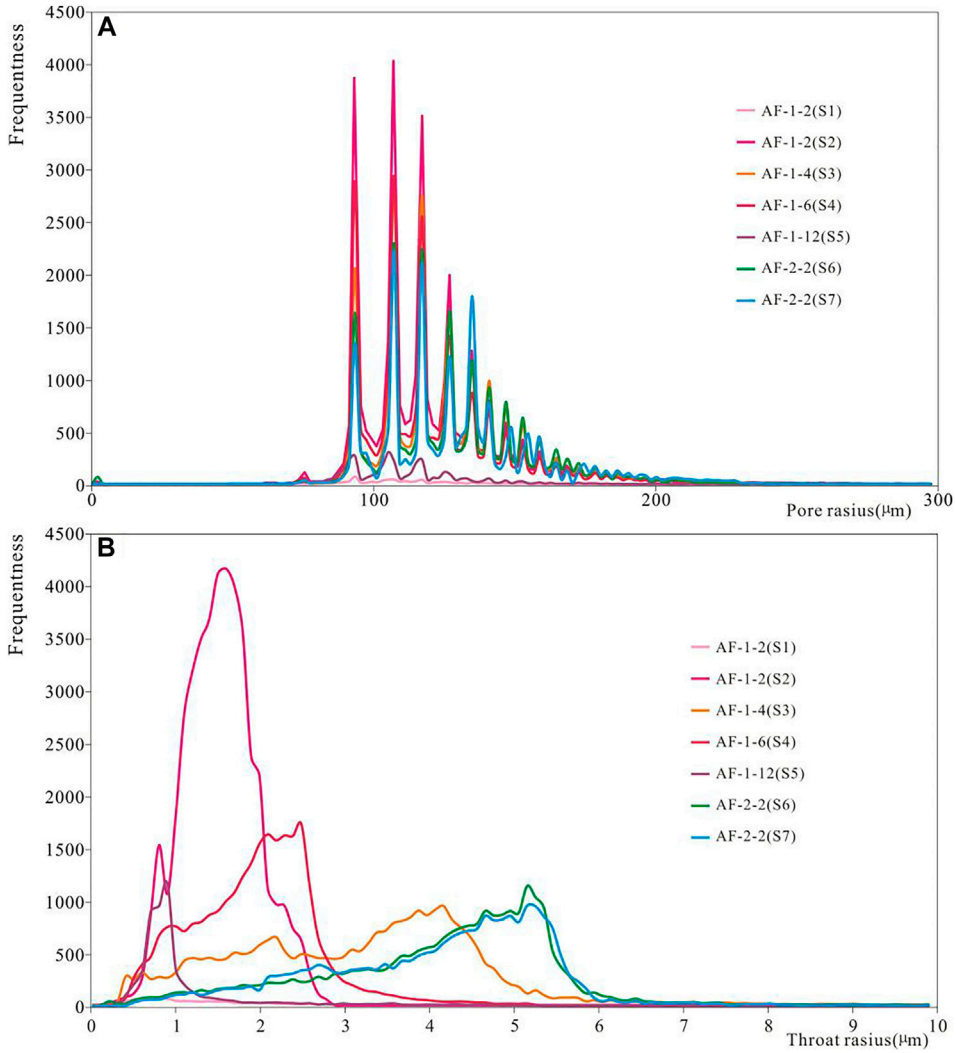

FIGURE 4 | Distribution curves of **(A)** pore radius and **(B)** throat radius from seven samples of the Huangliu sandstones in five wells from the AF-1 area and the AF-2 area, respectively.

cements in the AF-1 area mainly are composed of ankerite and siderite, while that of the AF-2 area are dominated by ferrocalcite and calcite (**Table 2**).

Early carbonate cements containing siderite, calcite, and dolomite mainly occur around grains as discontinuous coating and replace calcareous bioclastic (**Figure 5C**). A considerable amount of cements fill the intergranular pores as assemblage texture, or partly replace feldspar grains (**Figures 5D,E**; **Figure 6E**). The precipitation of ferrocalcite, symbolizing mesogenetic cements, are detected as glow dull red under CL and present as pore-filling and replacing grains (**Figures 5D,E**; **Figure 6D**), with a content of 0.3–1.0 vol% and 1.2–2.3 vol% in the AF-1 area and the AF-2 area, respectively (**Table 2**). The late carbonate cements principally include ankerite and siderite and are mostly distributed in the AF-1 area (**Table 2**). With coarser crystallinity and rhombohedron shape, ankerite generally fill intergranular pores and dissolved pores, or replace early cements (**Figure 6A**), with a fraction up to 7.1 vol% in the AF-1 area (**Table 2**). Unlike early analogue, late siderite exhibit better crystallinity and is relatively abundant in the AF-1 area, occurring as pore-filling constituent in dissolved pores or intermixing with clay minerals as hybrid agglomerate (**Figure 6C**). The coarser crystallinity implies an indicator of high-temperature genesis for siderite and ankerite.

4.2.2.2 Siliceous Cements

By observation of SEM, the overgrowth of euhedral microquartz can be detected on the surface of quartz grains (**Figure 6B**), and pore-filling aggregates of authigenic microquartz coexisting with authigenic filiform illite or I/S mixed-layer are also found (**Figures 7C,D**). Macroquartz cements and well-developed overgrowth are rarely observed, which indicate that the intensity of siliceous cementation is fairly weaker in the

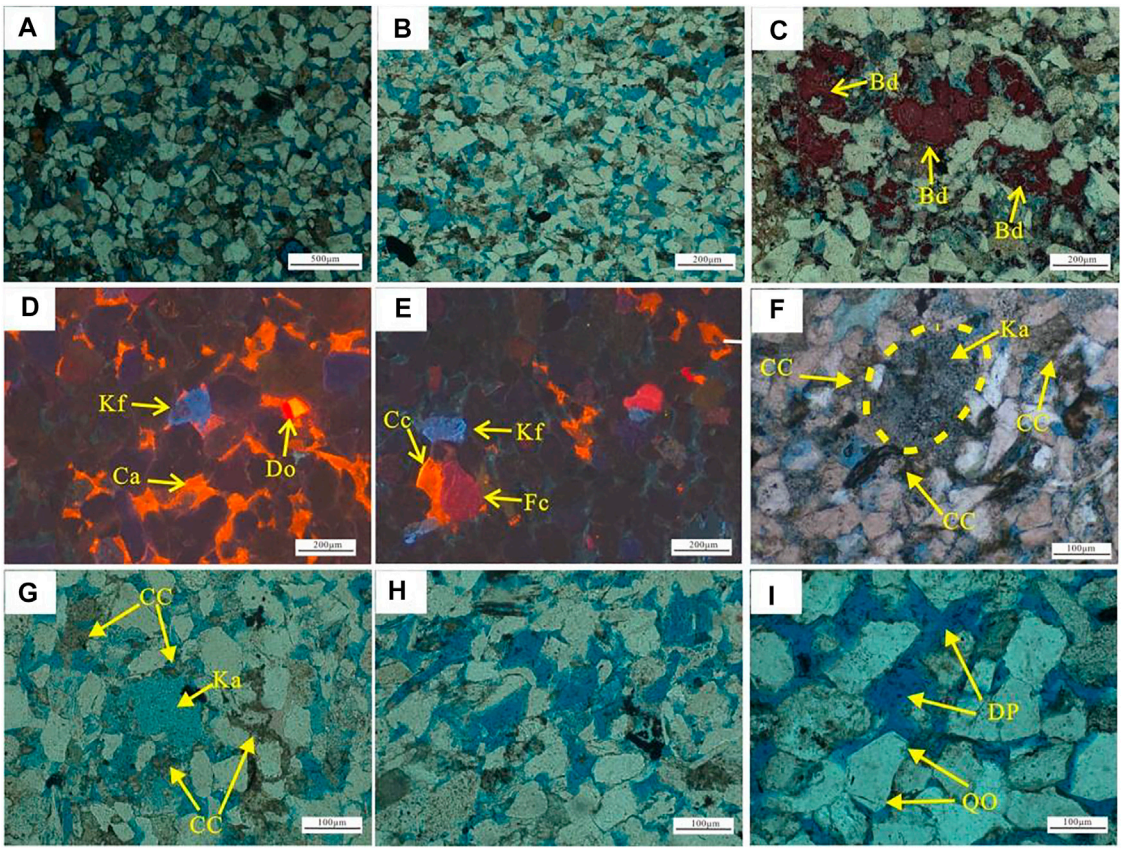

FIGURE 5 | Photomicrographs showing diagenetic characteristics of the Huangliu sandstones. **(A)** Well AF-2–1, 2,977.15 m, primary pores are well developed, and the types of particles contacts are dominated by line-point and planar. **(B)** Well AF-1–2, 3,040.96 m, weak compaction and dissolution pores are distributed widely. **(C)** Well AF-1–2, 2,992.16 m, biodetritus (Bd) are replaced by early carbonate cements. **(D)** Well AF-2–2, 3,134.16 m, calcite (Ca), dolomite (Do), and K-feldspar (Kf) fill intergranular pores. **(E)** Well AF-2–2, 3,067.64 m, the ferrocalcite (Fc) replace calcite (Ca) partly, and K-feldspar (Kf) are dissolved to some extent. **(F)** Well AF-1–2, 2,981.15 m, kaolinite (Ka) caused by feldspar dissolution exist in dissolved pores, and carbonate cements (CC) block pores and throats. **(G)** Well AF-1–2, 2,987.93 m, sandstones encounter strong dissolution, and related residual kaolinite and carbonate precipitation disperse in pore-throats. **(H)** Well AF-1–2, 3,047.09 m, feldspar grains are strongly dissolved to form large pores and enlarge intergranular pores. **(I)** Well AF-2–4, 3,215.5 m, fewer residues are left in dissolution pores (DP), and quartz overgrowth (QO) develops on detrital quartz.

TABLE 2 | Volume fraction of carbonate cements in the Huangliu sandstones.

Well	Calcite	Ferrocalcite	Dolomite	Ankerite	Siderite	Carbonate cements
		Average value (minimum to maximum value) φ_B/%				
AF-1–12	0.2 (0.1–0.3)	0.3 (0.1–0.5)	0.7 (0.5–1.0)	4.8 (2.5–6.3)	1.9 (1.2–3.6)	8.1 (6.2–11.1)
AF-1–14	0.3 (0.1–0.4)	0.3 (0.1–0.4)	0.6 (0.5–0.9)	3.4 (2.2–4.9)	1.7 (1.0–2.2)	6.9 (4.4–8.6)
AF-1–2	0.2 (0.1–0.5)	0.4 (0.1–0.6)	0.8 (0.5–1.5)	4.4 (2.2–5.3)	1.8 (0.9–2.5)	7.8 (5.1–9.8)
AF-1–4	0.2 (0.1–0.4)	0.7 (0.2–1.0)	0.7 (0.6–0.9)	5.1 (3.6–6.2)	1.4 (0.8–2.1)	8.8 (5.8–10.1)
AF-1–6	0.2 (0.1–0.5)	1.0 (0.2–1.4)	0.9 (0.6–1.7)	5.8 (4.6–7.1)	1.7 (1.0–2.4)	9.5 (7.3–12.2)
AF-2–1	0.2 (0.1–0.3)	1.3 (0.4–1.7)	0.6 (0.2–0.9)	0.5 (0.1–0.8)	0.8 (0.6–1.4)	3.2 (1.8–4.9)
AF-2–2	0.3 (0.1–0.4)	2.3 (1.1–3.5)	0.3 (0.1–0.5)	0.4 (0.2–0.7)	0.5 (0.2–0.8)	3.6 (1.9–5.1)
AF-2–4	0.2 (0.1–0.5)	2.2 (0.8–4.7)	0.2 (0.1–0.3)	0.2 (0.1–0.4)	0.2 (0.1–0.3)	2.8 (1.6–5.7)
AF-2–8	0.3 (0.1–0.4)	1.2 (0.5–1.5)	0.8 (0.3–1.2)	0.4 (0.2–0.6)	0.6 (0.2–1.0)	3.1 (1.9–4.5)

Huangliu sandstones. Conventionally, siliceous cementation shows higher sensibility to high temperature (Osborne and Swarbrick, 1999); nevertheless, the authigenic quartz and quartz overgrowth are determined in trace amount (<0.5 vol %) to minor amount (0.5–1.2 vol%). Previous studies demonstrate that weaker quartz overgrowth is closely related to the restriction of overpressure (Osborne and Swarbrick, 1999; Bloch et al., 2002).

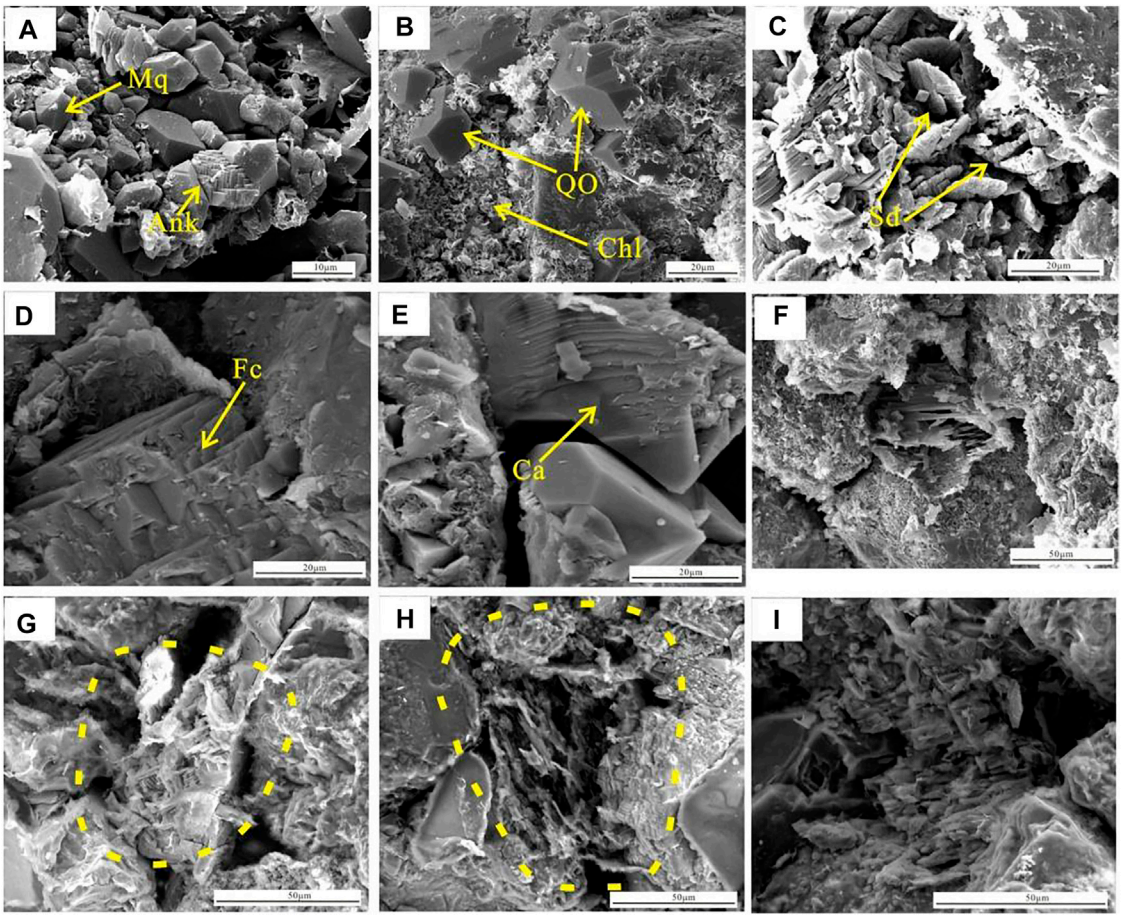

FIGURE 6 | Typical SEM photographs of diagenetic alterations in the Huangliu sandstones. **(A)** Well AF-1–6, 2,875.68 m, ankerite (Ank) and microquartz (Mq) exist in intergranular pores. **(B)** Well AF-1–12, 2,710.46 m, microquartz overgrowth develop on quartz grain with authigenic chlorite (Chl). **(C)** Well AF-1–6, 2,874.82 m, discus shape siderite (Sd) fill in dissolved pores. **(D)** Well AF-2–1, 3,004.12 m, ferrocalcite generate between particles and replace feldspar. **(E)** Well AF-2–1, 2,996.28 m, the intergranular space is taken up by calcite, and the cementation is partly corroded. **(F)** Well AF-1–4, 2,869.85 m, feldspar is subjected to heavy dissolution. **(G)** Well AF-1–2, 2,990.78 m, K-feldspar is dissolved and filiform illite exsit in pores and throats. **(H)** Well AF-1–3, 2,907.12 m, the feldspar is corroded and complex micropores develop. **(I)** Well AF-2–1, 3,110.38 m, K-feldspar is leached partly.

4.2.3 Authigenic Clay Minerals

The examination of XRD and SEM indicate that authigenic clay minerals in the Huangliu sandstones mainly contain illite, kaolinite, chlorite, and I/S mixed-layer. The AF-1 area presents higher relative contents of illite and kaolinite but extremely lower relative content of chlorite (**Figure 8**). The AF-2 area is dominated by higher relative fraction of chlorite and relatively lower relative proportion of kaolinite and illite (**Figure 8**).

The content of illite in the AF-1 area (51–62 wt% of total clay fraction) is obviously higher than that of the AF-2 area (18–31 wt% of total clay fraction) (**Figure 8**). The illite chiefly occur as filling-pores and blocking throats with a fibrous or pore-bridging form (**Figures 6G, 7D**), and in some places, surround grains as a flocculent grain-coating (**Figure 7C**). Controlled by high geothermal gradient, smectite disappear at a shallower burial depth, and thus can be rarely detected. The samples close to diapir show higher proportion of illite (90–95%) within a well-ordered I/S mixed-layer.

As identified by XRD, the kaolinite of the AF-1 area occurs with a fairly higher content (21–26% of total clay fraction) than that of the AF-2 area (12–16% of total clay fraction) (**Figure 8**). Detected by SEM, authigenic kaolinite commonly occur as pore-filling nature with vermiform or booklet texture (**Figures 7E,F**). In some cases, the kaolinite interlace with authigenic illite and chlorite, implying that they may have a genesis link. The extensive replacements of feldspar by authigenic kaolinite demonstrate that the dissolution acts as a significant developing mechanism for authigenic kaolinite (**Figures 5F,G**).

The chlorite contents in the AF-1 area range from trace to 8% of total clay fraction (**Figure 8**). By contrast, the chlorite in the AF-2 area presents obviously well-developed, accounting for 27–32%, total clay fraction (**Figure 8**). The authigenic chlorite display as needle-shaped or leaf-like platelets and generally surround particles as coating, or exist in intergranular pores (**Figures 7A,B**). The authigenic

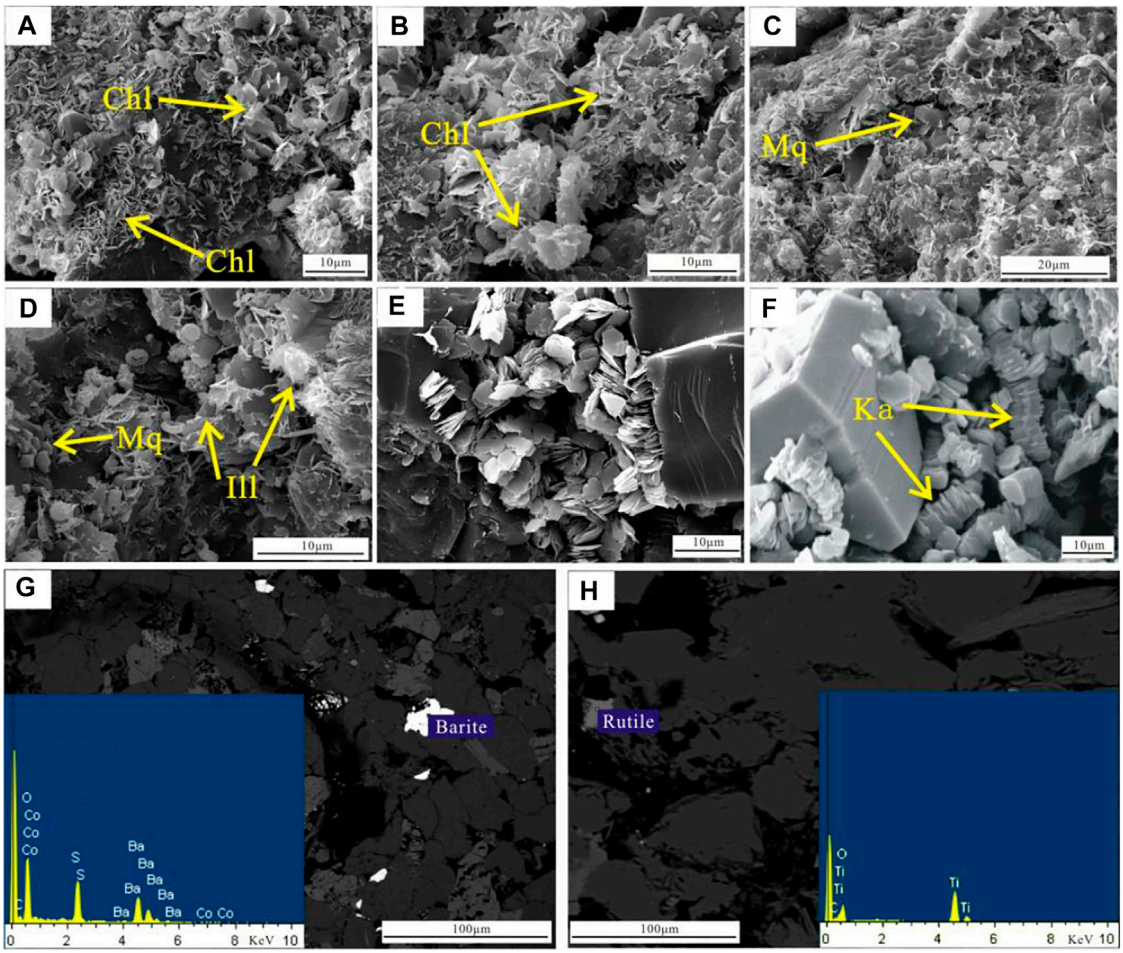

FIGURE 7 | Images of SEM and EMPA of authigenic clay minerals and hydrothermal minerals in the Huangliu sandstones. **(A)** Well AF-2–1, 3,042.12 m, needle-shaped and foliated chlorite present on particle surface. **(B)** Well AF-2–8, 3,082.65 m, needle-shaped chlorite wrap the surface of particle. **(C)** Well AF-1–12, 2,712.75 m, filamentous and foliaceous illite cover feldspar grain and microquartz (Mq) are encircled by illite and chlorite aggregate. **(D)** Well AF-1–12, 2,706.58 m, foliaceous and threadlike illite fill intergranular pores, and microquartz grains are surrounded by authigenic illite and chlorite. **(E)** Well AF-1–6, 2,861.32 m, abundant plate shape authigenic kaolinite fill interparticle space. **(F)** Well AF-1–4, 2,867.44 m, vermiform authigenic kaolinite exist in dissolved pore. **(G)** Well AF-1–6, 2,861.54 m, authigenic hydrothermal mineral of barite is detected. **(H)** Well AF-1–12, 2,709.71 m, hydrothermal mineral of rutile is found.

micoquartz partly develop on chlorite coating (**Figure 6B**), implying that chlorite rim formed before early quartz overgrowth. In addition, some microquartz are enclosed by pore-filling chlorite in dissolved pores, indicating that authigenic chlorite also has a late-period genesis (**Figures 7C,D**). Authigenic chlorite exert a non-negligible control on reservoir quality, and the significance of chlorite grain-coating on preserving primary porosity has been documented by numerous publications (Bloch et al., 2002; Taylor et al., 2010).

4.2.4 Dissolution

Based on thin section and SEM, the Huangliu sandstones have experienced severe dissolution, especially in the AF-1 area (**Figures 6F–I**). K-feldspar, plagioclase, and unstable lithic fragments constitute main material basis for multistage corrosion caused by multiple medium including mixed water, organic acids and CO_2-rich fluid (**Figures 5G–I**). Abundant moldic pores and oversized dissolved pores are mostly filled with vermicular stacked pseudohexagonal kaolinite (**Figures 7E,F**) and mixed assemblage of late-stage carbonate cements (**Figures 6A,C**), evidently revealing strong intensity of corrosion. By pore-count data from casting thin section, the visual dissolved porosities account for 46–48% of total porosities in the AF-1 area. In the AF-2 area, the dissolution strength appears relatively weaker, with a secondary porosity proportion of 19–22%. The honeycomb texture of partially dissolved feldspar, the marginal erosion with poorly defined boundaries of particles, and the incomplete corrosion for early cements all support a scenario of moderately to poorly dissolved status for investigated sandstones in the AF-2 area (**Figure 6I**), simultaneously with minor residues in the dissolved cavities (**Figure 5I**).

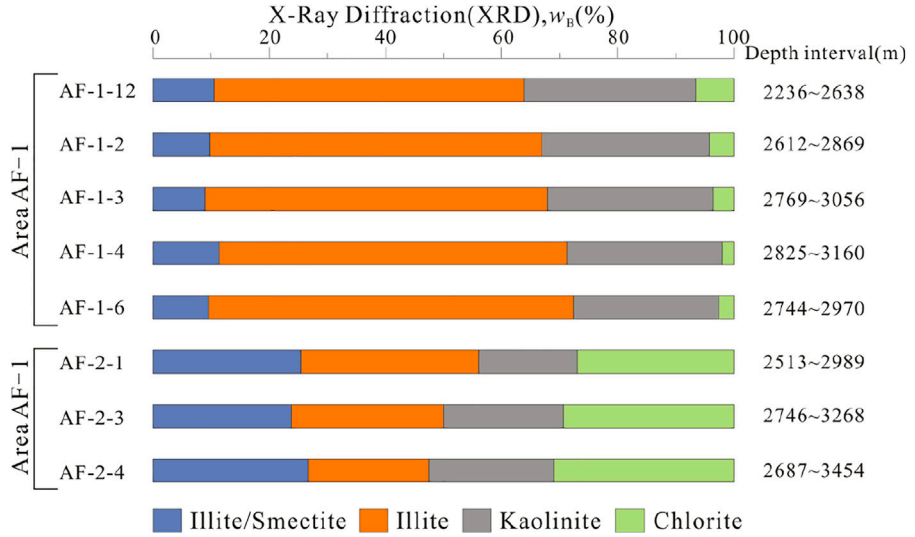

FIGURE 8 | Relative contents of clay minerals within the Huangliu sandstones from eight wells in the AF-1 area and the AF-2 area.

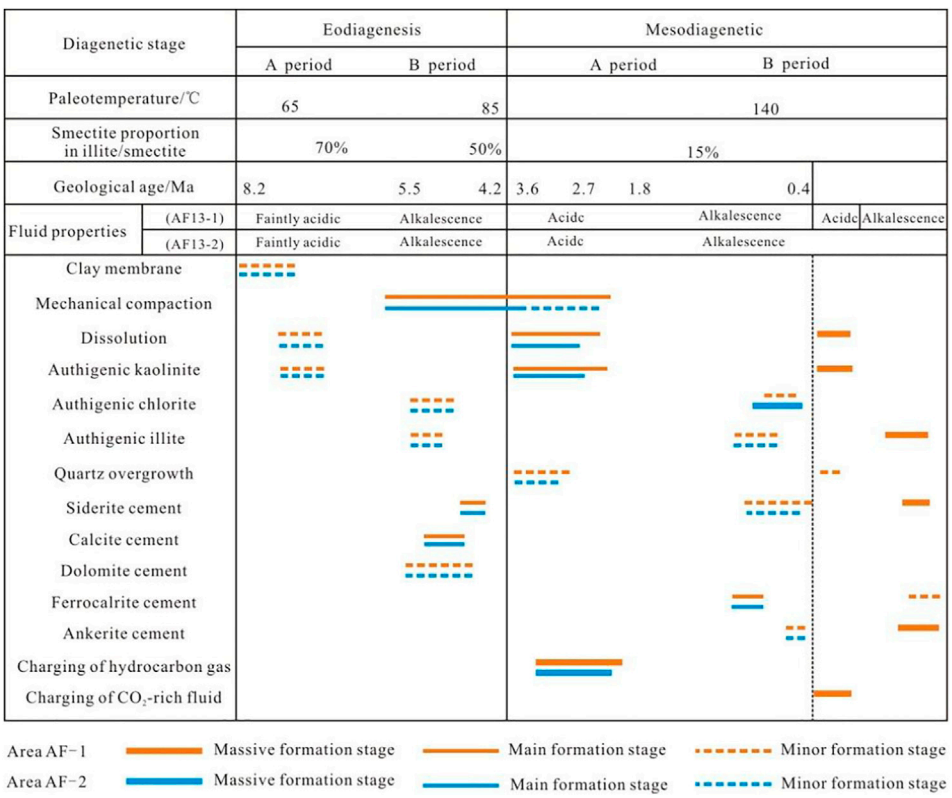

FIGURE 9 | Diagenetic sequence of the Huangliu sandstones in the AF-1 area and the AF-2 area.

4.2.5 Authigenic Hydrothermal Minerals

Determined by EPMA, the authigenic hydrothermal minerals of barite ($BaSO_4$) and rutile (TiO_2) are recognized in some intervals of the AF-1 area, and account for trace to 0.3 vol% of whole rock composition, with euhedral crystals mainly existing in intergranular pores (**Figures 7G,H**). Although exerting a minor influence on reservoir quality, the barite and rutile are suggested as an important indicator for occurrence of thermal fluid activity under high-temperature setting (Shi et al., 2014).

5 DISCUSSION

5.1 Heterogeneity of Diagenetic Phase and Paragenesis Sequence

The integrated analyses of authigenic minerals, petrologic structure and pore microstructure suggest that the AF-1 area mainly reach B-period of mediate diagenetic stage, while the AF-2 area mostly are maintained in the A-period of mediate diagenetic stage (**Figure 9**), as defined by Ying et al. (2003). This is also evidenced by thermal evolution indicators: 1) the AF-1 area present higher R_o value (0.88–1.4%) than that of the AF-2 area (0.58–1.05%); 2) the homogenization temperatures of fluid inclusion in the AF-1 area are higher than that in the AF-2 area on the whole; 3) the fraction of illite in I/S mixed-layer is 90–95% in the AF-1 area, with a lower range of 80–90% in the AF-2 area.

The intervals of the Huangliu sandstones in the AF-1 area (2700–2900 m) are shallower than that of the AF-2 area (2900–3100 m), whereas the diagenetic stages are contradictory to the equivalent depths. Previous studies suggest that the Huangliu sandstones have experienced overpressure, which can restrict diagenetic intensity to some extent (Duan et al., 2018). In addition, the AF-1 area suffered multistage thermal fluid activity, which elevated geothermal gradient dramatically and contributed to advanced diagenetic stage in the AF-1 area (Hao et al., 2000).

According to petrographic texture relationship, sequential order of authigenic minerals and burial history, the paragenetic sequence of the Huangliu sandstones are summarized as **Figure 9**. The AF-1 and AF-2 areas experience analogous paragenetic sequence of eodiagenesis and early stage of mesogenesis, and the relative onset timing are reconstructed as **Figure 9**. In addition, during late mesogenetic stage, the AF-1 area suffered multistage CO_2 charging, which caused significant modifications of paragenesis in the AF-1 area: 1) large-scale dissolution of feldspar particles; 2) extensive conversion of clay minerals, and 3) major precipitation of carbonate cements.

5.2 Overpressure Intensity and Occurring Timing

The effect of overpressure on preservation of primary porosity has been evidenced by considerable a few of literature (Gluyas and Cade, 1997; Bloch et al., 2002; Taylor et al., 2010). Fluid overpressure decreases VES to various extent, and therefore lightens the load of sediments during ongoing compaction, which acts as a chief mechanism for resisting mechanical compaction and maintaining intergranular porosity (Bloch et al., 2002; Nguyen et al., 2013). Under parallel depositing setting and buried depth, the potential of porosity preservation have positive correlation with the magnitude of overpressure (Gluyas and Cade, 1997). In addition, the early occurring timing of fluid overpressure is generally favorable for the capacity against compaction (Paxton et al., 2002).

Overpressure prevails in the Huangliu sandstones and play a significant role in compaction trend and primary porosity preservation. In this study, the contacting index (CI), as defined by Liang et al. (2011) and illustrated by **Formula 1**, is adopted to quantitatively assess the potential of overpressure on resistance to compaction, which is calculated by a function related to the various grain contact patterns conducted by thin section counting (Liang et al., 2011).

$$CI = (a + 1.5ab + 2b + 3c + 4d)/(a + ab + b + c + d) \quad (1)$$

(Liang et al., 2011) Notation: a-number of points contact; ab-number of point-line contacts; b-number of line contacts; c-number of concave and convex contacts; d-number of suture contacts.

According to Liang et al. (2011), CI is classified by three categories: weak compaction (1.0–1.5), medium compaction (1.5–2.5), strong compaction (>2.5). For detailed comparison, this research further subdivides medium compaction into grade I medium compaction (CI ~ 1.5–1.8) and grade II medium compaction (CI ~ 1.8–2.5). The CI values calculated show that the AF-1 area are dominated by grade I medium compaction and that of the AF-2 area almost fall into the scope of grade II, showing that the compaction of the AF-1 area is stronger than that of the AF-2 area (**Figure 10**). The tests data show the present-day strata pressure of the AF-1 area exceeds that of the AF-2 area (**Table 1**), which is inconsistent with the trend of compaction degree. Given the similar depositing environments, the occurring timing of overpressure should be considered to interpret the anomalous trend.

Considering the origin of overpressure, the modeling of interval transit time (ITT) for mudstone is suitable to estimate the occurring timing of the overpressure (Duan et al., 2018). The

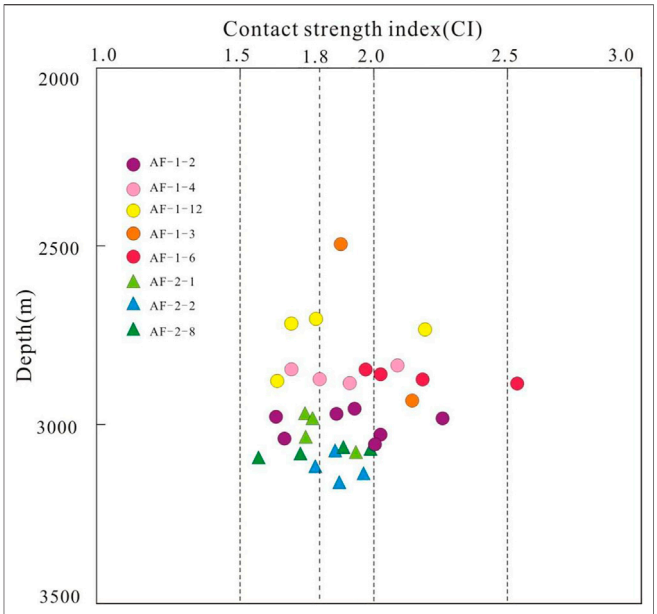

FIGURE 10 | The relationships of contact strength index (CI) vs. depth in eight wells from the AF-1 area and the AF-2 area.

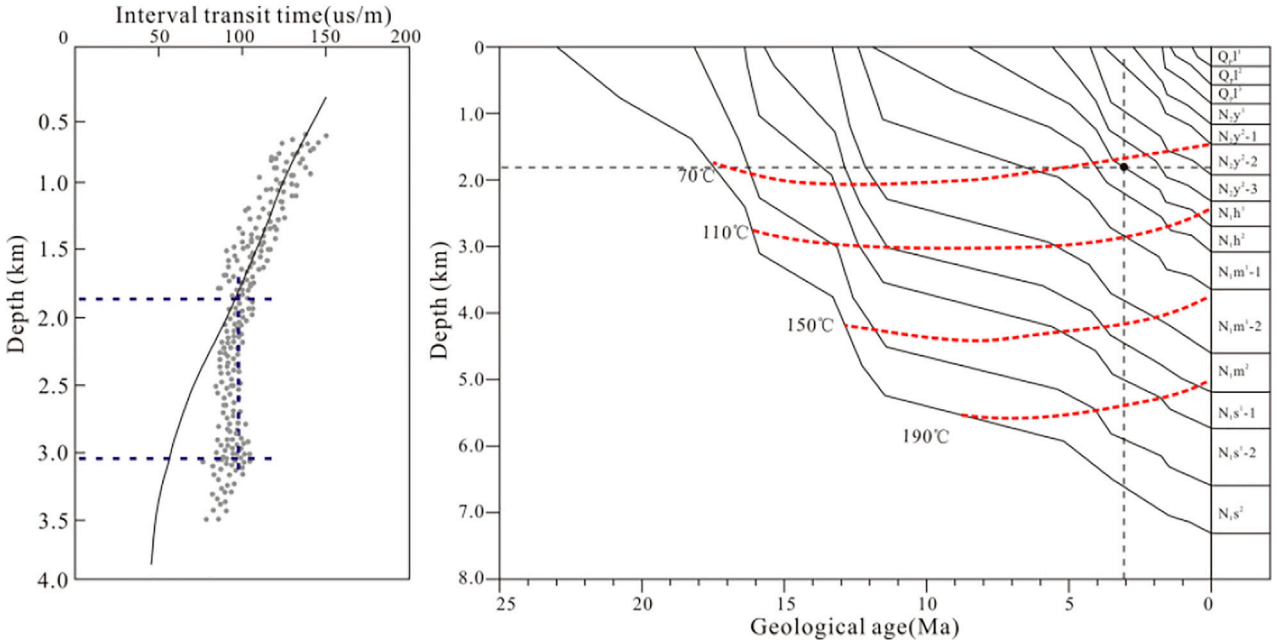

FIGURE 11 | Schematic diagram of the calculation theory about onset timing for overpressure in well AF-1–2.

ITT deviating toward normal compaction curve indicate that compacting process start to suffer overpressure, at which depth the overpressure occurred (Fu and Zhang, 1998). The depth of deviating point is projected on the corresponding burial history, and synchronously the occurring timing of overpressure is determined (**Figure 11**). With the computed results, the occurring time of overpressure in the AF-2 area (2.8–3.0 Ma) are earlier than the AF-1 area (2.7–2.8 Ma), which is considered as the significant reason to explain weaker compaction in the AF-2 area. During late diagenetic stage, the multiphase episodic intrusion of CO_2 enhance the pressure field and geothermal gradient in the AF-1 area, which is mainly responsible to higher present-day strata pressure. The overpressure can work for preserving primary porosity only at the moment when grains are still bearing ongoing compaction (Paxton et al., 2002), and therefore a late-period strengthening of overpressure subsequent to fully compacted status has only minor contribution to preserving primary porosity. This argument provides a more valuable insight into elucidating a higher ratio of primary porosity and weaker compaction degree but with deeper burial depth in the AF-2 area compared with the AF-1 area.

5.3 Multi-Phase Cementation and Dissolution in Diverse Diagenetic System

During dissolution–reprecipitation reactions, the diagenetic system exhibiting open or closed geochemical constrains determine the scale of mass transport, resulting in various by-products and authigenic minerals assemblages, and profoundly influencing reservoir quality (Bjørlykke and Jahren, 2012; Yuan et al., 2015).

In early diagenesis, the near-surface dissolution of silicate minerals induced by mixed marine and meteoric waters commonly occur in open geological system, which are mainly controlled by the flowing rate of pore fluid and undersaturation degree of solution (Bjørlykke and Jahren, 2012). The Huangliu sandstones deposit in lowstand systems tract (Huang et al., 2019), which provide preferable conditions for mixed water dissolution (Morad et al., 2000). Although the early dissolution is weaker and lasts a short duration because of lower temperature and H^+ concentration, the open geochemical system contribute to enhancing dissolved porosity.

With abnormally high geothermal gradient, the thermal decarboxylation of adjacent mudstone began to generate organic acids at an earlier time in the Dongfang district (Barth and Bjørlykke, 1993; Hao et al., 2000). Fluid inclusion geochemistry and kinetics simulation of hydrocarbon generation indicate that initial timing of hydrocarbon charging occurred at 3.7 Ma approximately in the Huangliu sandstones (Xie et al., 2012), and the expulsion of accompanying organic acids generally are proposed to arise before or during hydrocarbon charging (Surdam et al., 1989). The above research show that the overpressure of the Huangliu sandstones formed at 2.7–3.0 Ma, and appeared posterior to organic acids filling, implying that organic acids dissolution predated overpressure. Before overpressure forming, the progressive compaction provided driving force for advective and diffusive mass transport of pore fluids, which served as an open or semi-open geochemical system for mass transport (Bjørlykke, 2014). Consequently, the residual by-products induced by organic acid leaching can be discharged to various

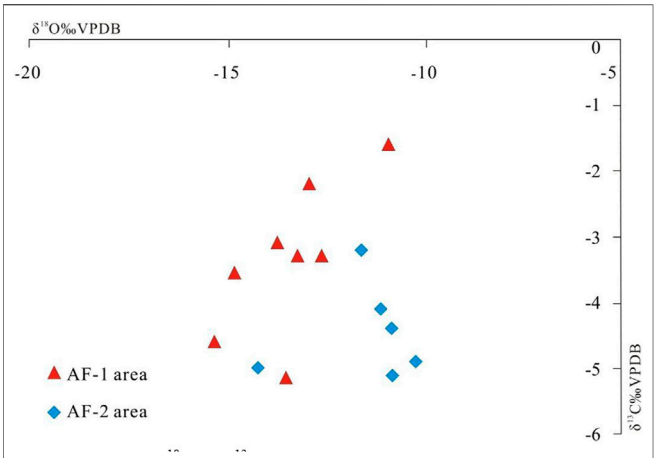

FIGURE 12 | Scatter diagram of δ18 O vs. δ13C for calcite cements in the Huangliu sandstones.

degree, which enhanced dissolved porosities to some extent for the Huangliu sandstones (Yuan et al., 2015).

The overpressure is evidenced as a significant event for kinetically restricting the producing efficiency of organic acids and forming a geochemically closed diagenetic system (Hao et al., 2007; Bjørlykke, 2014). Therefore, the dissolution was constrained and became weaker gradually. The previous publication documented that overpressure could restrain clay minerals transformation, causing that the yield of metal cations acting as the reactant for precipitation of carbonate cements were restricted (Meng et al., 2012). In addition, overpressure can enhance the solubility of carbonate in aqueous solution, and thus hinder the precipitation of carbonate cements (Duan et al., 2018). These factors proposed above are mainly responsible for the lower contents of carbonate cements in the AF-2 area (**Table 2**). The fluid inclusions of ferrocalcite cements in the AF-2 area show a range of homogenization temperature of 72–98°C, implying that the carbonate cements of the AF-2 area mainly formed during the mesodiagenesis and were consistent with the main temperature span (80–120°C) of organic acids expulsion proposed by Surdam et al. (1989). A lighter value of $\delta^{13}C$ suggest that the ferrocalcite cements mainly belong to the precipitation induced by organic acids dissolution (**Figure 12**).

Earlier research revealed that CO_2-rich thermal fluid from the underlying beds invaded the AF-1 area (Hao et al., 2000), which occurred as a pattern of multiphase episodic vertical injection from about 0.4 Ma (Xie et al., 2012) and was evidenced by high content of CO_2 (**Table 1**). The AF-1 area suffer extreme influence from CO_2 filling, and rarely affected traces are found in the AF-2 area (Duan et al., 2020).

The CO_2 charging exert serious control on diagenetic evolution and reservoir quality and thus raise more concern from petroleum geologists (Fu et al., 2016; Duan et al., 2020). The dissolution of unstable minerals induced by CO_2 charging was widely reported (Watson et al., 2004; Wigley et al., 2012). When expelling into saline aquifers, the CO_2 dissolved in pore fluid and broke geochemical equilibrium, resulting in a weak-acid setting (Wigley et al., 2012). In the Huangliu sandstones, the overpressure enhanced the solubility of CO_2 and thus increased the acidity, and thermal fluid migration induced anomalously high temperature, which greatly facilitated dissolution (Fu et al., 2016). The dissolved pores natures characterized by abundant oversized pores and high-proportioned secondary porosity visibly indicate large-scale dissolution in the AF-1 area.

The potential of enhancing porosity by dissolution mainly depend on the byproduct distribution released from feldspar grains, which are constrained by the properties of geochemically diagenetic system (Yuan et al., 2015). Based on material equilibrium, the most effective dissolution for enhancing net porosity is therefore expected in sandstones which are exposed to a geochemically open system and can freely discharge by-products and authigenic minerals (Nedkvitne and Bjørlykke, 1992). With the sealed effect by overpressure, the diagenetic environment is generally considered to be a geochemically closed system and removing large quantities of solute become extreme difficulty (Wilkinson et al., 1997). The hydraulic fracture was demonstrated to be a pressure leak-off point in the overpressure strata of the Central Graben in the North Sea, from which the fluid could migrate through the top seal (Wilkinson et al., 1997). The leak-off point induced an open system and allowed dissolution products to migrate dynamically, which was beneficial to enhance secondary porosity (Wilkinson et al., 1997).

In the diapir, steep-dipping fractures associated with diapir evolution act as significant channels for fluid migration and mass transfer, from which the reactive material and production can discharge (Hao et al., 2000; Yuan et al., 2019) (**Figure 2A**). Based on gas accumulation and diagenetic progress, the thermal fluid migration in diapir was proposed to have an episodic nature (Hao et al., 2000). When CO_2-rich thermal fluid injected the Huangliu sandstones along fractures, the feldspar, lithic fragments and carbonate cements suffered extensive dissolution. The dissolution products can be transferred out of reservoir by fluid migration, which can enhance storage potential (Qie et al., 2021). During the intervals of thermal fluid upwelling, the diagenetic system was in a semi-closed or even closed state, and the flow rate of pore fluid decelerated drastically and the efficiency of mass transfer became extremely lower (Yuan et al., 2015). In addition, the temperature and pressure of formation decreased accordingly (Hao et al., 2000). The extensive dissolution and advanced conversion of clay minerals provided abundant Ca^{2+}, Mg^{2+} and Fe^{2+}, which combined with high content of CO_3^{2-} to form a large amount of late-period carbonate cements (Duan et al., 2018), damaging permeability seriously (**Figure 13C**). The heavier $\delta^{13}C$ value of ankerite and siderite in the AF-1 area indicated the carbonate cements were mainly associated with inorganic CO_2 (**Figure 12**).

The multistage thermal fluid induced cumulative diagenetic process characterized by the overlap of multiphase dissolution and subsequent precipitation (Jansa and Noguera Urrea, 1990; Xue et al., 2021). During the expulsion of CO_2-rich fluid, the diagenetic system was relatively open and the dissolution had a constructive effect for porosity, which was suggested the main

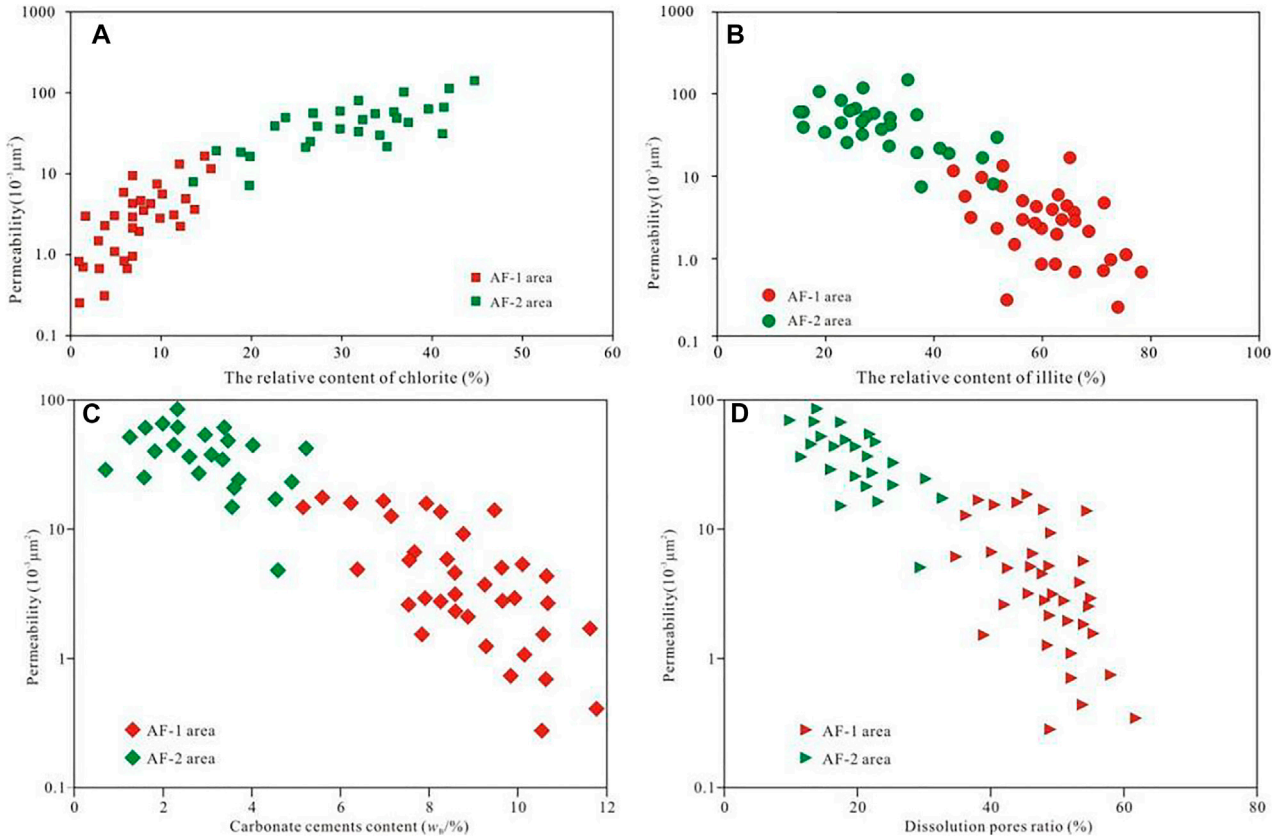

FIGURE 13 | Correlation between permeability and **(A)** relative content of chlorite, **(B)** relative content of illite, **(C)** carbonate cements content, and **(D)** dissolution pores ratio in the Huangliu sandstones.

mechanism to interpret higher total porosities of the AF-1 area than that of the AF-2 area despite experiencing stronger compaction.

In some case, considerable amount of dissolved pores are poorly connected to pores network due to the blocking of remnants and cements (Lai et al., 2017; Liu et al., 2020). The multiphase, the high contents of carbonate cements act as occluding material to block pore-throats (**Figures 5F,G**), resulting in a set of microstructures characterized by smaller throats size and poor interconnectivity (**Figure 6H**), which is one of main reasons for low permeability in the AF-1 area (**Figure 13D**). Moreover, the massive dissolution and the assemblage of authigenic minerals can modify pore-size distribution, minerals surface feature and pores geometry, complicating the seepage regime and decreasing penetrability significantly (Dutton and Loucks, 2010; Chen et al., 2021).

Well-connected primary pores tend to have large throat size contributing to permeability, whereas secondary pores and micropores connected by confined pore-throats are disadvantageous to permeability (Dutton and Loucks, 2010). The AF-2 area suffered little effect from intensive dissolution of CO_2 charging. As a result, the lower contents of carbonate cements and weaker dissolution intensity protect more primary pores and present a higher proportion of primary porosity and medium-permeability (**Figure 13D**).

5.4 Different Evolution Tendency of Clay Minerals

Clay minerals in sandstone reservoirs occur with varied assembling patterns and relative amounts, which are mainly controlled by transformation process influenced by combined factors including temperature, pressure and fluid properties (Bjørlykke, 1998; Meng et al., 2012). For the Huangliu sandstones, the complicated diagenetic setting with HTHP and thermal fluid exert considerable control on clay transformation and distribution.

Temperature is a crucial factor for illitization of smectite, and furthermore, the compositional trends in I/S mixed-layer are taken as an indicator of geothermal distribution (Bühmann, 1992). Generally, the illitization of smectite presents an increasing rate with rising geothermal gradient (Meng et al., 2012). Influenced by thermal anomaly induced by thermal fluid in the AF-1 area, the illitization of smectite accelerated markedly (Hao et al., 2000). In contrast, with the effect of suppressing dehydration for smectite by increasing pressure, the overpressure can restrain the transformation from smectite

to illite (Colten-Bradley, 1987). Furthermore, overpressure can limit the source of K^+ by restricting dissolution of K-feldspar, which also act as a retarder for transformation of smectite to illite by limiting reacting materials (Chuhan et al., 2001). In addition, with an earlier onset timing of overpressure, the AF-2 area experienced stronger restraint and had lower intensity of illitization of smectite accordingly.

The distribution of authigenic chlorite is controlled by thermal history, fluid property, and ferromagnesian grains (Bahlis and De Ros, 2013). With similar depositional setting and burial experience, the AF-2 area present obviously higher contents of authigenic chlorite than the AF-1 area, implying differential transformation process. Authigenic chlorite in the Huangliu sandstones occur predominately as pore-lining and rosette pattern, which are similar to the Santos sandstones in eastern Brazil described by Bahlis and De Ros (2013). Different from progressive transformation of smectite coatings in the Santos sandstones, smectite coatings and volcanic rock fragments are absent in the Huangliu sandstones, indicating that smectitic precursor rarely act as dominating source for authigenic chlorite (Bahlis and De Ros, 2013). With weak alkaline environment, the transformation of kaolinite integrated ferroan carbonates to chlorite is considered as a significant way to form chlorite (Meng et al., 2012). From thermodynamics perspective, chlorite is unstable and particularly prone to transforming to kaolinite under high temperature and acidic condition (Meng et al., 2012) **(Eq. 2)**. During the late period, weakly acidic and high temperature conditions caused by a thermal fluid induced major dissolution of chlorite (Meng et al., 2012; He et al., 2020). Therefore, the key diagenetic event of late-stage transformation mainly contributes to reducing chlorite in the AF-1 area, which is consistent with the measured results. As verified by quite a few of papers, chlorite coating and pore-lining chlorite play a positive role in inhibiting quartz cementation and restraining compaction (Bloch et al., 2002; Taylor et al., 2010; Mohammed et al., 2021). The measured permeability of the Huangliu sandstones are positively correlated with the amount of chlorite, indicating constructive significance of authigenic chlorite on reservoir quality (**Figure 13A**).

With massive dissolution of feldspar induced by CO_2 charging, a considerable amount of authigenic kaolinite are still detained in the AF-1 area, despite a part of authigenic kaolinite are transported out of dissolved pores by fluid expulsion and consumed by illitization of kaolinite (Chuhan et al., 2001; Yuan et al., 2019). As one of major pore-filling constituents, the residual kaolinite with vermicular and booklets habits develop abundant micropores (Lai et al., 2015). The micropores apparently add a lesser amount of total storage volume, and nevertheless, the microporous texture intertwining with pseudomatrix can enhance the tortuosity of seepage channels and tend to have poor interconnectivity, which also exacerbate permeability in the AF-1 area (Worden and Morad, 2003; Lai et al., 2015).

Apart from illitization of smectite, the illitization of kaolinite is also a major genesis for authigenic illite (Chuhan, et al., 2000). In the AF-2 area, the overpressure suppressed the dissolution of K-feldspar, which distinctly decreased the concentration of K^+. In addition, the closed diagenetic system limit the transfer of K^+ (Yuan et al., 2019). In a closed system, the appropriate thermodynamic condition for precipitation of authigenic illite is a temperature range of 120–140°C (Chuhan, et al., 2001). The homogenization temperature of fluid inclusion shows a mainstream interval of 85–115°C. The conditions mentioned above restrict the reactants and diagenetic setting for illite precipitation in the AF-2 area. In the AF-1 area, the significant diagenetic event of thermal fluid expulsion caused intensive dissolution of K-feldspar and thus provided abundant K^+ and kaolinite for illite precipitation **Eq. (3)** (Chuhan, et al., 2001). Furthermore, the thermal fluid activities can evoke vertical transfer of potassium along fractures in overpressure sequence, therefore enhancing illitization of kaolinite (Yuan et al., 2019). The thermal anomaly heightened the formation temperature in the AF-1 area with a paleogeothermal interval of 123–165°C, improving illitization of kaolinite largely (Duan, et al., 2020). Consequently, the favorable geochemical and thermodynamic conditions yielded abundant authigenic illite in the AF-1 area which exceeded the AF-2 area obviously. As for the AF-1 area, the widespread fibrous and pore-bridging illite aggregation blocked throats and damaged permeability significantly (Lai et al., 2017) (**Figure 13B**). More seriously, in a deeply buried sequence with high temperature, fibrous illite decrease permeability by several orders of magnitude (Ajdukiewicz and Lander, 2010). Based on data of physical properties, the permeability presented a negative correlation with the amount of illite (**Figure 13B**). In contrast, the poorly developed authigenic illite in the AF-2 area contributed to seepage behavior and permeability.

$$\begin{aligned} Fe_{3.5}Mg_{3.5}Al_6Si_6O_{20}(OH)_{16}\ (\text{Chloride}) + 14\,H^+ \\ = 3\,Al_2Si_2O_5(OH)_4\,(\text{Kaolinite}) + 3.5\,Fe^{2+} \\ + 3.5\,Mg^{2+} + 9H_2O, \end{aligned} \tag{2}$$

$$\begin{aligned} Al_2Si_2O_5(OH)_4\,(\text{Kaolinite}) + KAlSiO_3 \\ = KAl_3Si_3O_{10}(OH)_2\ (\text{Illite}) + 2\,SiO_2 + H_2O. \end{aligned} \tag{3}$$

5.5 Two Different Mechanisms of Reservoirs Development

The physical properties of reservoir are generally governed by integrated attributes of depositional characteristics and subsequent diagenetic modifications (Mansurbeg et al., 2008). The elements relevant to deposition including detrital composition, sedimentary structure, grain size and amount of matrix determine original pores system (Ozkan et al., 2011). After depositing, a wide variety of diagenetic modifications of compaction, dissolution and cementation significantly control reservoirs quality and heterogeneity (Morad et al., 2000). In particular, exceptional diagenetic modifications induced by extreme diagenetic setting such as HPHT and CO_2 charging can even obscure the depositional imprints (Ozkan et al., 2011). As for

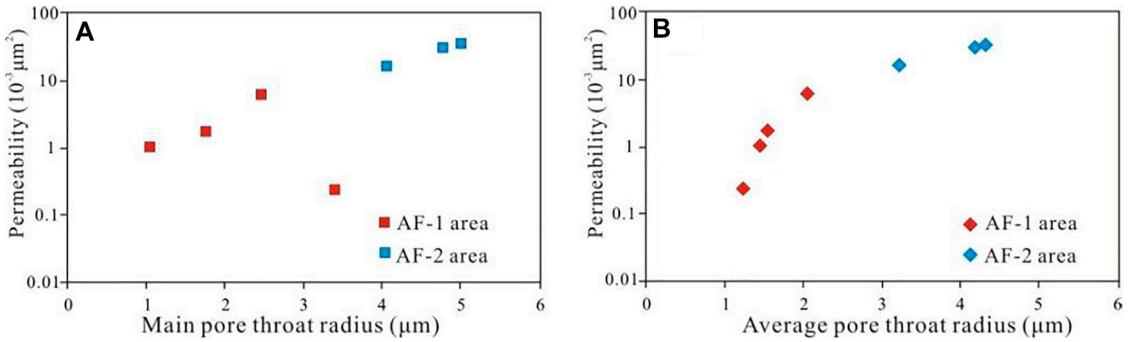

FIGURE 14 | Cross plot of permeability vs. main throat radius **(A)** and average throat radius **(B)** in the Huangliu sandstones.

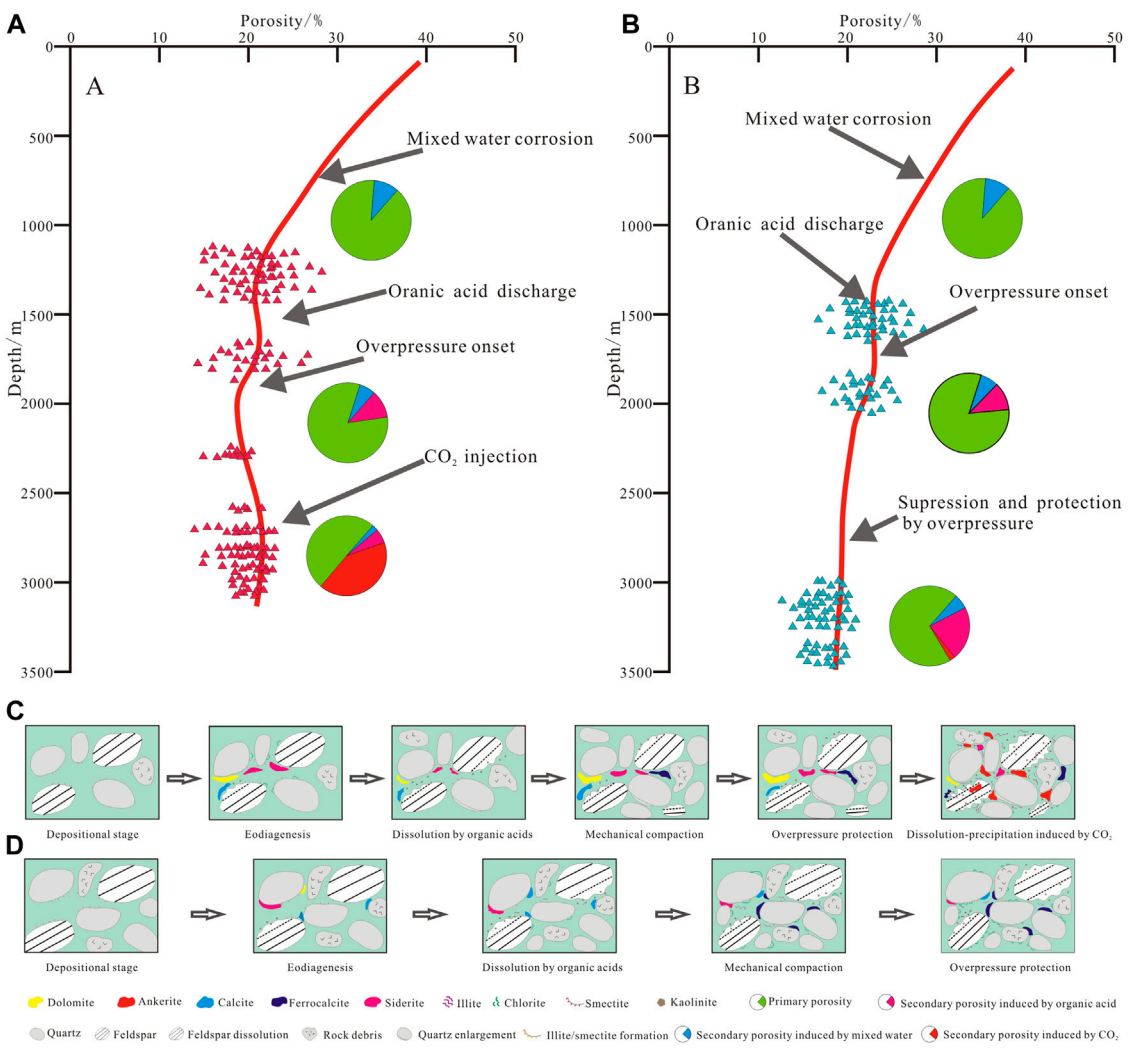

FIGURE 15 | Trend of porosity evolution with depth in the AF-1 area **(A)** and the AF-2 area **(B)**, and diagenetic evolution of the Huangliu sandstones in the AF-1 area **(C)** and the AF-2 area **(D)** in the Dongfang district.

the Huangliu sandstones, it appeared analogous depositional features between the AF-1 and AF-2 areas. However, controlled by different diagenetic environments, the AF-1 area and the AF-2 area presented variable diagenetic histories, resulting in a wide variety of spatial and temporal distribution of diagenetic alterations across the two areas (Ozkan et al., 2011).

As a routinely employed method for porosity prediction, porosity versus depth curves tend to have considerable limitation in greater depths where sandstones experience stronger diagenetic degree, such as extensive dissolution and cementation (Taylor et al., 2010). Especially, in the extreme cases exposed to HPHT and CO_2 dissolution, the conventional porosity versus depth trends are essentially meaningless for porosity prediction (Taylor et al., 2010). Therefore, for such diagenetically heterogeneous sandstones, the porosity modeling dependent on depths variation should be revalued based on extreme diagenetic events.

Based on synthetical analysis of diagenetic alterations, we establish two patterns of porosity evolution for the Huangliu sandstones to deepen understanding of development mechanism of reservoirs (**Figure 15**). Previous to overpressure occurrence, considerable amount of intergranular volumes were lost due to progressive compaction. In early period, the dissolution associated with mixed water increased porosity slightly. The medium-term corrosion by organic acid can add a certain number of dissolved porosities. The mechanical compaction was retarded when overpressure occurred, and thus more primary porosities were preserved and the downward trend of porosity became slower, especially in the AF-2 area with an earlier onset timing of resistance to compaction (**Figure 15**). Restrained by overpressure, the dissolution derived by organic acids was limited and so was cementation strength, which restricted secondary porosity but retained more primary porosities. During late diagenetic stage in the AF-1 area, dissolved porosities were improved dramatically by CO_2 injection, resulting in higher proportion of secondary pores and abnormal rise of average porosity (**Figure 15**). With lesser influence from CO_2 dissolution and chiefly suppressed by overpressure, the AF-2 area had a gentle variation of porosity–depth curve and higher primary porosity, though showed marginally lower porosity than the AF-1 area in the mass.

As a critical factor to characterize seepage performance, permeability is considered as a function of porosity and connectivity of individual pore and predominantly controlled by pore-throat size (Dutton and Loucks, 2010). While causing a wide variation of porosities, diagenetic modifications also act as a crucial factor for reconstructing original pores network, controlling pore-throat size and consequently determining permeability (Dutton and Loucks, 2010). An evident positive relationship existing between throat size and permeability, indicated that the variations of permeability were dominantly controlled by the distribution of throat size (**Figure 14**). The higher contents of carbonate cements and authigenic illite caused by CO_2 injection under anomalously high temperature blocked throats severely, resulting in a rapid loss of permeability for the Huangliu sandstones in the AF-1 area (**Figures 13B,C**). With stronger influence by unremitting overpressure and lesser impact from CO_2 charging in the AF-2 area, the authigenic illite and kaolinite were suppressed largely, and the cementation intensity of carbonate cements was also restricted, which prevented serious damage for permeability (**Figures 13B,C**).

With intensive diagenetic modifications, the AF-1 area present higher average porosity due to massive dissolution. However, the redistribution of secondary porosities and simultaneous authigenic minerals deteriorated permeability with one or two orders of magnitude lower than the AF-2 area restricted effectively by overpressure (Aase et al., 1996) (**Figure 13**). As for the Huangliu sandstones with similar depositional features, the spatial and temporal differentiation of diagenetic settings resulted in two obviously diverse patterns of diagenesis-driven evolution pathways and development mechanisms, and formed two categories of reservoirs (**Figure 15**). Considering significant impact by anomalous diagenetic environments, it is quite essential to link the combined modes of anomalous diagenetic conditions with diagenetic evolution and development mechanism for the sandstones characterized by HPHT and CO_2 injection. This study enhances our understanding on the formation mechanism of sandstone reservoirs under anomalous diagenetic conditions, and provides important geological reference for reservoirs prediction in HPHT sequences in the Yinggehai Basin and other basins worldwide with similar geological conditions.

6 CONCLUSION

1) The reservoir characteristics of the Huangliu sandstones present regional diversity. The AF-1 area is characterized by high proportion of secondary porosity and medium porosity to low permeability, while the AF-2 area is dominated by primary porosity and medium porosity to medium permeability. The determination of rate-controlled porosimetry indicate that the AF-1 area show distinctly lower throat sizes than that of the AF-2 area overall, which is mainly responsible for low permeability in the AF-1 area.
2) In the AF-1 area, the later occurrence time of overpressure cause stronger compaction intensity and major loss of primary porosity. The multistage invasion of CO_2-rich thermal fluids in the late stage induced intense corrosion of feldspar grains and enhanced secondary porosity significantly, and therefore improved total porosity. Meanwhile, extensive CO_2 dissolution caused abundant precipitations including carbonate cements and authigenic illite in a closed diagenetic system, which leaded to the blocking of throats and lowering of seepage capacity.
3) For the AF-2 area, earlier onset of overpressure restrained mechanical compaction obviously, and further retarded the corrosion of organic acid, which preserved more primary porosities. Rarely influenced by CO_2 filling, the CO_2 dissolution and carbonate cementation were markedly weaker. The conversions of clay minerals were restrained significantly because of overpressure and lesser impact by thermal fluids. The weaker diagenetic strength prevented heavy deterioration for reservoir quality, especially for permeability.
4) The onset timing of overpressure, the distribution trend of high temperature and the scope of influence by CO_2 filling vary significantly between the AF-1 and AF-2 areas. The diagenesis strength and diagenetic modifications show distinct difference due to the integrated impact of anomalous diagenetic environments, which cause two types of diagenetic evolution

pathways, forming two development patterns and exhibiting different reservoir types for the Huangliu sandstones.

DATA AVAILABILITY STATEMENT

The original contributions presented in the study are included in the article/Supplementary Material; further inquiries can be directed to the corresponding authors.

AUTHOR CONTRIBUTIONS

XL and MF are responsible for the idea and writing of this manuscript; SZ, XM, YL, XD, YZ, and TS are responsible for the data interpretations.

FUNDING

The author(s) disclosed receipt of the following financial support for the research, authorship, and/or publication of this article: National Science and Technology Major Project (Grant No. KJ125ZDXM07LTD02ZJ11).

ACKNOWLEDGMENTS

We would like to acknowledge staff of the State Key Laboratory of Oil and Gas Reservoir Geology and Development, Zhanjiang Branch Company of CNOOC, for their contribution of data and valuable discussion, which significantly improved the quality of the manuscript.

REFERENCES

Ajdukiewicz, J. M., and Lander, R. H. (2010). Sandstone Reservoir Quality Prediction: The State of the Art. *Bulletin* 94 (8), 1083–1091. doi:10.1306/intro060110

Aase, N. E., Bjørkum, P. A., and Nadeau, P. H. (1996). The Effect of Grain-Coating Microquartz on Preservation of Reservoir Porosity. *Bulletin* 80 (10), 1654–1673. doi:10.1306/64EDA0F0-1724-11D7-8645000102C1865D

Bahlis, A. B., and De Ros, L. F. (2013). Origin and Impact of Authigenic Chlorite in the Upper Cretaceous Sandstone Reservoirs of the Santos Basin, Eastern Brazil. *Pet. Geosci.* 19, 185–199. doi:10.1144/petgeo2011-007

Barth, T., and Bjørlykke, K. (1993). Organic Acids from Source Rock Maturation: Generation Potentials, Transport Mechanisms and Relevance for Mineral Diagenesis. *Appl. Geochem.* 8, 325–337. doi:10.1016/0883-2927(93)90002-X

Bjørlykke, K. (1998). Clay Mineral Diagenesis in Sedimentary Basins - a Key to the Prediction of Rock Properties. Examples from the North Sea Basin. *Clay Min.* 33, 15–34. doi:10.1180/000985598545390

Bjørlykke, K., and Jahren, J. (2012). Open or Closed Geochemical Systems during Diagenesis in Sedimentary Basins: Constraints on Mass Transfer during Diagenesis and the Prediction of Porosity in Sandstone and Carbonate Reservoirs. *Bulletin* 96 (12), 2193–2214. doi:10.1306/04301211139

Bjørlykke, K. (2014). Relationships between Depositional Environments, Burial History and Rock Properties. Some Principal Aspects of Diagenetic Process in Sedimentary Basins. *Sediment. Geol.* 301, 1–14. doi:10.1016/j.sedgeo.2013.12.002

Bloch, S., Lander, R. H., and Bonnell, L. (2002). Anomalously High Porosity and Permeability in Deeply Buried Sandstone Reservoirs: Origin and Predictability. *Bulletin* 86 (2), 301–328. doi:10.1306/61EEDABC-173E-11D7-8645000102C1865D

Bühmann, C. (1992). Smectite-to-illite Conversion in a Geothermally and Lithologically Complex Permian Sedimentary Sequence. *Clays Clay Minerals* 40 (1), 53–64. doi:10.1346/CCMN.1992.0400107

Bukar, M., Worden, R. H., Bukar, S., and Shell, P. (2021). Diagenesis and its Controls on Reservoir Quality of the Tambar Oil Field, Norwegian North Sea. *Energy Geosci.* 2 (1), 10–31. doi:10.1016/j.engeos.2020.07.002

Chen, G. B., Li, T., Yang, L., Zhang, G. H., Li, J. W., and Dong, H. J. (2021). Mechanical Properties and Failure Mechanism of Combined Bodies with Different Coal-Rock Ratios and Combinations. *J. Min. Strata Control Eng.* 3 (2), 023522. doi:10.13532/j.jmsce.cn10-1638/td.20210108.001

Chuhan, F. A., Bjorlykke, K., and Lowrey, C. J. (2001). Closed-system Burial Diagenesis in Reservoir Sandstones: Examples from the Garn Formation at Haltenbanken Area, Offshore Mid-Norway. *J. Sediment. Res.* 71 (1), 15–26. doi:10.1306/041100710015

Chuhan, F. A., Bjørlykke, K., and Lowrey, C. (2000). The Role of Provenance in Illitization of Deeply Buried Reservoir Sandstones from Haltenbanken and North Viking Graben, Offshore Norway. *Mar. Petroleum Geol.* 17, 673–689. doi:10.1016/S0264-8172(00)00014-3

Colten-Bradley, V. A. (1987). Role of Pressure in Smectite Dehydration--Effects on Geopressure and Smectite-To-Illite Transformation. *Bulletin* 71 (11), 1414–1427. doi:10.1306/703C8092-1707-11D7-8645000102C1865D

Di Primio, R., and Neumann, V. (2008). HPHT Reservoir Evolution: a Case Study from Jade and Judy Fields, Central Graben, UK North Seafields, Central Graben, UK North Sea. *Int. J. Earth Sci. Geol. Rundsch)* 97, 1101–1114. doi:10.1007/s00531-007-0206-y

Dong, S., Zeng, L., Lyu, W., Xia, D., Liu, G., Wu, Y., et al. (2020). Fracture Identification and Evaluation Using Conventional Logs in Tight Sandstones: A Case Study in the Ordos Basin, China. *Energy Geosci.* 1 (3–4), 115–123. doi:10.1016/j.engeos.2020.06.003

Duan, W., Li, C.-F., Chen, X.-G., Luo, C.-F., Tuo, L., and Liu, J.-Z. (2020). Diagenetic Differences Caused by Gas Charging with Different Compositions in the XF13 Block of the Yinggehai Basin, South China Sea. *Bulletin* 104 (4), 735–765. doi:10.1306/06191917331

Duan, W., Li, C.-F., Luo, C., Chen, X.-G., and Bao, X. (2018). Effect of Formation Overpressure on the Reservoir Diagenesis and its Petroleum Geological Significance for the DF11 Block of the Yinggehai Basin, the South China Sea. *Mar. Petroleum Geol.* 97, 49–65. doi:10.1016/j.marpetgeo.2018.06.033

Dutton, S. P., and Loucks, R. G. (2010). Diagenetic Controls on Evolution of Porosity and Permeability in Lower Tertiary Wilcox Sandstones from Shallow to Ultradeep (200-6700m) Burial, Gulf of Mexico Basin, U.S.A. *Mar. Petroleum Geol.* 27, 69–81. doi:10.1016/j.marpetgeo.2009.08.008

Folk, R. L. (1980). *Petrology of Sedimentary Rocks*. Austin, TX: Hemphill Publishing Company, 182.

Fu, G., and Zhang, F. Q. (1998). A Method for Analyzing the Paleo-Pressure Sealing Ability of Poorly Compacted Shale Barrier with the Use of Acoustic Logging Data. *Oil Geophys. Prospect.* 33 (6), 812–818. doi:10.13810/j.cnki.issn.1000-7210.1998.06.014

Fu, M.-y., Song, R.-c., Xie, Y.-h., Zhang, S.-n., Gluyas, J. G., Zhang, Y.-z., et al. (2016). Diagenesis and Reservoir Quality of Overpressured Deep-Water Sandstone Following Inorganic Carbon Dioxide Accumulation: Upper Miocene Huangliu Formation, Yinggehai Basin, South China Sea. *Mar. Petroleum Geol.* 77, 954–972. doi:10.1016/j.marpetgeo.2016.08.005

Gluyas, J., and Cade, C. A. (1997). Prediction of Porosity in Compacted Sands. *Reserv. Qual. Predict. Sandst. carbonatesAAPG Mem.* 69, 19–27. doi:10.1306/M69613C2

Grant, N. T., Middleton, A. J., and Archer, S. (2014). Porosity Trends in the Skagerrak Formation, Central Graben, United Kingdom Continental Shelf: The Role of Compaction and Pore Pressure History. *Bulletin* 98 (6), 1111–1143. doi:10.1306/10211313002

Hao, F., Li, S. T., and Gong, Z. S. (2000). Thermal Regime, Interreservoir Compositional Heterogeneities, and Reservoir-Filling History of the Dongfang Gas Field, Yinggehai Basin, South China Sea: Evidence for Episodic Fluid Injections in Overpressured Basins? *Bulletin* 84 (5), 607–626. doi:10.1306/C9EBCE69-1735-11D7-8645000102C1865D

Hao, F., Zou, H., Gong, Z., Yang, S., and Zeng, Z. (2007). Hierarchies of Overpressure Retardation of Organic Matter Maturation: Case Studies from

Petroleum Basins in China. *Bulletin* 91 (10), 1467–1498. doi:10.1306/05210705161

He, X., Zhang, P., He, G., Gao, Y., Liu, M., Zhang, Y., et al. (2020). Evaluation of Sweet Spots and Horizontal-Well-Design Technology for Shale Gas in the Basin-Margin Transition Zone of Southeastern Chongqing, SW China. *Energy Geosci.* 1 (3–4), 134–146. doi:10.1016/j.engeos.2020.06.004

Higgs, K. E., Zwingmann, H., Reyes, A. G., and Funnell, R. H. (2007). Diagenesis, Porosity Evolution, and Petroleum Emplacement in Tight Gas Reservoirs, Taranaki Basin, New Zealand. *J. Sediment. Res.* 77, 1003–1025. doi:10.2110/jsr.2007.095

Huang, Y., Yao, G., and Fan, X. (2019). Sedimentary Characteristics of Shallow-Marine Fans of the Huangliu Formation in the Yinggehai Basin, China. *Mar. Petroleum Geol.* 110, 403–419. doi:10.1016/j.marpetgeo.2019.07.039

Huang, Y., Yao, G., Zhou, F., and Wang, T. (2017). Impact Factors on Reservoir Quality of Clastic Huangliu Formation in Overpressure Diapir Zone, Yinggehai Basin, China. *J. Petroleum Sci. Eng.* 154, 322–336. doi:10.1016/j.petrol.2017.04.044

Jansa, L. F., and Noguera Urrea, V. H. (1990). Geology and Diagenetic History of Overpressured Sandstone Reservoirs, Venture Gas Field, Offshore Nova Scotia, Canada (1). *Bulletin* 74 (10), 1640–1658. doi:10.1306/0C9B2551-1710-11D7-8645000102C1865D

Lai, J., Wang, G., Chai, Y., Ran, Y., and Zhang, X. (2015). Depositional and Diagenetic Controls on Pore Structure of Tight Gas Sandstone Reservoirs: Evidence from Lower Cretaceous Bashijiqike Formation in Kelasu Thrust Belts, Kuqa Depression in Tarim Basin of West China. *Resour. Geol.* 65 (2), 55–75. doi:10.1111/rge.12061

Lai, J., Wang, G., Chai, Y., Xin, Y., Wu, Q., Zhang, X., et al. (2017). Deep Burial Diagenesis and Reservoir Quality Evolution of High-Temperature, High-Pressure Sandstones: Examples from Lower Cretaceous Bashijiqike Formation in Keshen Area, Kuqa Depression, Tarim Basin of China. *Bulletin* 101 (6), 829–862. doi:10.1306/08231614008

Lan, S. R., Song, D. Z., Li, Z. L., and Liu, Y. (2021). Experimental Study on Acoustic Emission Characteristics of Fault Slip Process Based on Damage Factor. *J. Min. Strata Control Eng.* 3 (3), 033024. doi:10.13532/j.jmsce.cn10-1638/td.20210510.002

Li, H. (2022). Research Progress on Evaluation Methods and Factors Influencing Shale Brittleness: A Review. *Energy Rep.* 8, 4344–4358. doi:10.1016/j.egyr.2022.03.120

Li, Y. (2021). Mechanics and Fracturing Techniques of Deep Shale from the Sichuan Basin, SW China. *Energy Geosci.* 2 (1), 1–9. doi:10.1016/j.engeos.2020.06.002

Li, Y., Zhou, D.-H., Wang, W.-H., Jiang, T.-X., and Xue, Z.-J. (2020). Development of Unconventional Gas and Technologies Adopted in China. *Energy Geosci.* 1 (1–2), 55–68. doi:10.1016/j.engeos.2020.04.004

Liang, J. S., Wang, Q., Hao, L. W., Tang, J., Liao, P., et al. (2011). Application of Diagenetic Facies Analysis to Reservoir Prediction in Deep Water Area of the Northern South China Sea: a Case Study from Baiyun Sag, Zhujiangkou Basin. *Acta Sedimentol. Sin.* 29 (3), 503–511. doi:10.14027/j.cnki.cjxb.2011.03.002

Liu, Y., Gao, M., and Zhao, H. (2020). Detection of Overlying Rock Structure and Identification of Key Stratum by Drilling and Logging Technology. *J. Min. Strata Control Eng.* 2 (2), 023038. doi:10.13532/j.jmsce.cn10-1638/td.2020.02.004

Luo, X., Dong, W., Yang, J., and Yang, W. (2003). Overpressuring Mechanisms in the Yinggehai Basin, South China Sea. *Bulletin* 87 (4), 629–642. doi:10.1306/10170201045

Mansurbeg, H., Morad, S., Salem, A., Marfil, R., El-ghali, M. A. K., Nystuen, J. P., et al. (2008). Diagenesis and Reservoir Quality Evolution of Palaeocene Deep-Water, Marine Sandstones, the Shetland-Faroes Basin, British Continental Shelf. *Mar. Petroleum Geol.* 25, 514–543. doi:10.1016/j.marpetgeo.2007.07.012

Meng, F. J., Xiao, L. H., Xie, Y. H., Wang, Z. F., Liu, J. H., Tong, C. X., et al. (2012). Abnormal Transformation of the Clay Minerals in Yinggehai Basin and its Significances. *Acta Sedimentol. Sin.* 30 (3), 469–476. doi:10.14027/j.cnki.cjxb.2012.03.005

Morad, S., Ketzer, J. M., and De Ros, L. F. (2000). Spatial and Temporal Distribution of Diagenetic Alterations in Siliciclastic Rocks: Implications for Mass Transfer in Sedimentary Basins. *Sedimentology* 47 (Suppl. 1), 95–120. doi:10.1046/j.1365-3091.2000.00007.x

Nedkvitne, T., and Bjørlykke, K. (1992). Secondary Porosity in the Brent Group (Middle Jurassic), Huldra Field, North Sea: Implication for Predicting Lateral Continuity of Sandstones? *Sepm Jsr* 62 (1), 23–34. doi:10.1306/D426787A-2B26-11D7-8648000102C1865D

Nguyen, B. T. T., Jones, S. J., Goulty, N. R., Middleton, A. J., Grant, N., Ferguson, A., et al. (2013). The Role of Fluid Pressure and Diagenetic Cements for Porosity Preservation in Triassic Fluvial Reservoirs of the Central Graben, North Sea. *Bulletin* 97 (8), 1273–1302. doi:10.1306/01151311163

Osborne, M. J., and Swarbrick, R. E. (1999). Diagenesis in North Sea HPHT Clastic Reservoirs - Consequences for Porosity and Overpressure Prediction. *Mar. Petroleum Geol.* 16, 337–353. doi:10.1016/S0264-8172(98)00043-9

Ozkan, A., Cumella, S. P., Milliken, K. L., and Laubach, S. E. (2011). Prediction of Lithofacies and Reservoir Quality Using Well Logs, Late Cretaceous Williams Fork Formation, Mamm Creek Field, Piceance Basin, Colorado. *Bulletin* 95 (10), 1699–1723. doi:10.1306/01191109143

Paxton, S. T., Szabo, J. O., and Ajdukiewicz, J. M. (2002). Construction of an Intergranular Volume Compaction Curve for Evaluating and Predicting Compaction and Porosity Loss in Rigid-Grain Sandstone Reservoirs. *Bulletin* 86 (12), 2047–2067. doi:10.1306/61EEDDFA-173E-11D7-8645000102C1865D

Qie, L., Shi, Y. N., and Liu, J. S. (2021). Experimental Study on Grouting Diffusion of Gangue Solid Filling Bulk Materials. *J. Min. Strata Control Eng.* 3 (2), 023011. doi:10.13532/j.jmsce.cn10-1638/td.20201111.001

Surdam, R. C., Crossey, L. J., Hagen, E. S., and Heasler, H. P. (1989). Organic-inorganic Interactions and Sandstone Diagenesis. *Bulletin* 73 (1), 1–23. doi:10.1306/703C9AD7-1707-11D7-8645000102C1865D

Santosh, M., and Feng, Z. Q. (2020). New Horizons in Energy Geoscience. *Energy Geosci.* 1 (1–2), A1–A2. doi:10.1016/j.engeos.2020.05.005

Sathar, S., and Jones, S. (2016). Fluid Overpressure as a Control on Sandstone Reservoir Quality in a Mechanical Compaction Dominated Setting: Magnolia Field, Gulf of Mexico. *Terra nova.* 28 (3), 155–162. doi:10.1111/ter.12203

Schmoker, J. W., and Gautier, D. L. (1988). Sandstone Porosity as a Function of Thermal Maturity. *Geol* 16, 1007–1010. doi:10.1130/0091-7613(1988)016<1007:spaafo>2.3.co;2

Shi, Z. Q., Wang, Y., and Jin, X. (2014). The Silurian Hydrothermal Clastic Reservoirs in Tarim Basin: Evidences, Mineral Assemblages and its Petroleum Geological Implications. *Oil Gas Geol.* 35 (6), 903–913. doi:10.11743/ogg20140617

Stricker, S., Jones, S. J., Sathar, S., Bowen, L., and Oxtoby, N. (2016). Exceptional Reservoir Quality in HPHT Reservoir Settings: Examples from the Skagerrak Formation of the Heron Cluster, North Sea, UK. *Mar. Petroleum Geol.* 77, 198–215. doi:10.1016/j.marpetgeo.2016.02.003

Taylor, T. R., Giles, M. R., Hathon, L. A., Diggs, T. N., Braunsdorf, N. R., Birbiglia, G. V., et al. (2010). Sandstone Diagenesis and Reservoir Quality Prediction: Models, Myths, and Reality. *Bulletin* 94 (8), 1093–1132. doi:10.1306/04211009123

Taylor, T. R., Kittridge, M. G., Bryndzia, L. T., and Fibonnell, L. M. (2015). Reservoir Quality and Rock Properties Modeling - Triassic and Jurassic Sandstones, Greater Shearwater Area, UK Central North Sea. *Mar. Petroleum Geol.* 65, 1–21. doi:10.1016/j.marpetgeo.2015.03.020

Tingay, M. R. P., Hillis, R. R., Swarbrick, R. E., Morley, C. K., and Damit, A. R. (2009). Origin of Overpressure and Pore-Pressure Prediction in the Baram Province, Brunei. *Bulletin* 93 (1), 51–74. doi:10.1306/08080808016

Wang, H., Shi, Z., Zhao, Q., Liu, D., Sun, S., Guo, W., et al. (2020). Stratigraphic Framework of the Wufeng-Longmaxi Shale in and Around the Sichuan Basin, China: Implications for Targeting Shale Gas. *Energy Geosci.* 1 (3–4), 124–133. doi:10.1016/j.engeos.2020.05.006

Wang, J., and Wang, X. L. (2021). Seepage Characteristic and Fracture Development of Protected Seam Caused by Mining Protecting Strata. *J. Min. Strata Control Eng.* 3 (3), 033511. doi:10.13532/j.jmsce.cn10-1638/td.20201215.001

Watson, M. N., Zwingmann, N., and Lemon, N. M. (2004). The Ladbroke Grove-Katnook Carbon Dioxide Natural Laboratory: A Recent CO2 Accumulation in a Lithic Sandstone Reservoir. *Energy* 29, 1457–1466. doi:10.1016/j.energy.2004.03.079

Wigley, M., Kampman, N., Dubacq, B., and Bickle, M. (2012). Fluid-mineral Reactions and Trace Metal Mobilization in an Exhumed Natural CO2 Reservoir, Green River, Utah. *Geology* 40, 555–558. doi:10.1130/G32946.1

Wilkinson, M., Darby, D., Haszeldine, R. S., and Couples, G. D. (1997). Secondary Porosity Generation during Deep Burial Associated with Overpressure Leak-Off: Fulmar Formation, United Kingdom Central Graben. *Bulletin* 81 (5), 803–813. doi:10.1306/522B484D-1727-11D7-8645000102C1865D

Wilkinson, M., Haszeldine, R. S., Fallick, A. E., Odling, N., Stoker, S. J., and Gatliff, R. W. (2009). CO2-Mineral Reaction in a Natural Analogue for CO2 Storage--Implications for Modeling. *J. Sediment. Res.* 79, 486–494. doi:10.2110/jsr.2009.052

Worden, R. H., and Morad, S. (2003). Clay Minerals in Sandstones: Controls on Formation, Distribution and Evolution. *Int. Assoc. Sedimentol. Spec. Publ.* 34, 1–41. doi:10.1002/9781444304336.ch1

Xie, Y. H., Zhang, Y. Z., Li, X. S., Zhu, J. C., Tong, C. X., Zhong, Z. H., et al. (2012). Main Controlling Factors and Formation Models of Natural Gas Reservoirs with High-Temperature and Overpressure in Yinggehai Basin. *Acta Pet. Sin.* 33 (4), 601–609. doi:10.7623/syxb201204009

Xue, F., Liu, X. X., and Wang, T. Z. (2021). Research on Anchoring Effect of Jointed Rock Mass Based on 3D Printing and Digital Speckle Technology. *J. Min. Strata Control Eng.* 3 (2), 023013. doi:10.13532/j.jmsce.cn10-1638/td.20201020.001

Yang, J. X., Luo, M. K., Zhang, X. W., Huang, N., and Hou, S. J. (2021). Mechanical Properties and Fatigue Damage Evolution of Granite under Cyclic Loading and Unloading Conditions. *J. Min. Strata Control Eng.* 3 (3), 033016. doi:10.13532/j.jmsce.cn10-1638/td.20210510.001

Ying, F. X., He, D. B., Long, Y. M., Wang, K. Y., Long, Y. M., Lin, X. S., et al. (2003). *SY/T5477, the Division of Diagenetic Stages in Clastic Rocks (Petroleum Industry Criterion in P.R.C.)*. Beijing: Petroleum Industry Press. (in Chinese).

Yoshida, M., and Santosh, M. (2020). Energetics of the Solid Earth: An Integrated Perspective. *Energy Geosci.* 1 (1–2), 28–35. doi:10.1016/j.engeos.2020.04.001

Yuan, G., Cao, Y., Gluyas, J., Li, X., Xi, K., Wang, Y., et al. (2015). Feldspar Dissolution, Authigenic Clays, and Quartz Cements in Open and Closed Sandstone Geochemical Systems during Diagenesis: Typical Examples from Two Sags in Bohai Bay Basin, East China. *Bulletin* 99 (11), 2121–2154. doi:10.1306/07101514004

Yuan, G., Cao, Y., Schulz, H.-M., Hao, F., Gluyas, J., Liu, K., et al. (2019). A Review of Feldspar Alteration and its Geological Significance in Sedimentary Basins: From Shallow Aquifers to Deep Hydrocarbon Reservoirsficance in Sedimentary Basins: From Shallow Aquifers to Deep Hydrocarbon Reservoirs. *Earth-Science Rev.* 191, 114–140. doi:10.1016/j.earscirev.2019.02.004

Zhang, B., Shen, B., and Zhang, J. (2020). Experimental Study of Edge-Opened Cracks Propagation in Rock-like Materials. *J. Min. Strata Control Eng.* 2 (3), 033035. doi:10.13532/j.jmsce.cn10-1638/td.20200313.001

Zhang, J., Ju, Y., and Zhang, Q. (2019). Low Ecological Environment Damage Technology and Method in Coal Mines. *J. Min. Strata Control Eng.* 1 (1), 013515. doi:10.13532/j.jmsce.cn10-1638/td.2019.02.005

Zhao, Z., Wu, K., Fan, Y., Guo, J., Zeng, B., and Yue, W. (2020). An Optimization Model for Conductivity of Hydraulic Fracture Networks in the Longmaxi Shale, Sichuan Basin, Southwest China. *Energy Geosci.* 1 (1–2), 47–54. doi:10.1016/j.engeos.2020.05.001

Zheng, H., Zhang, J., and Qi, Y. (2020). Geology and Geomechanics of Hydraulic Fracturing in the Marcellus Shale Gas Play and Their Potential Applications to the Fuling Shale Gas Development. *Energy Geosci.* 1 (1–2), 36–46. doi:10.1016/j.engeos.2020.05.002

Zuo, J., Yu, M., and Hu, S. (2019). Experimental Investigation on Fracture Mode of Different Thick Rock Strata. *J. Min. Strata Control Eng.* 1 (1), 013007. doi:10.13532/j.jmsce.cn10-1638/td.2019.02.008

Conflict of Interest: XL was employed by the the research institute of Henan Oilfield Company, YL was employed by the research institute of Zhanjiang Branch of CNOOC, and YZ was employed by the Southwest Oil and Gas field Company of Petro China Company Limited.

The remaining authors declare that the research was conducted in the absence of any commercial or financial relationships that could be construed as a potential conflict of interest.

Publisher's Note: All claims expressed in this article are solely those of the authors and do not necessarily represent those of their affiliated organizations, or those of the publisher, the editors, and the reviewers. Any product that may be evaluated in this article, or claim that may be made by its manufacturer, is not guaranteed or endorsed by the publisher.